# University of Padova

Department of Information Engineering


*Master Thesis in Telecommunication Engineering*

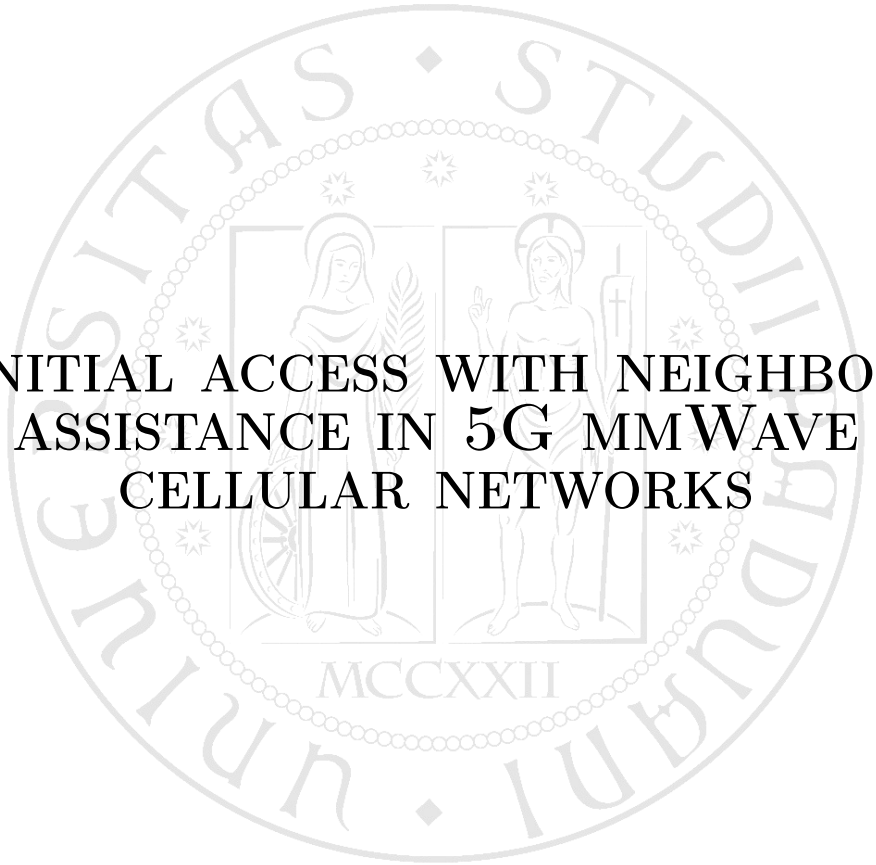

# Initial access with neighbor assistance in 5G mmWave cellular networks


*Master candidate*

**Filippo Cappellaro**

*Supervisor*

**Prof. Stefano Tomasin**


---


30 September 2019

Academic Year 2018/2019

To Chiara, Maria, and Martina

# Contents

**Abstract**

The advent of fifth-generation (5G) communications has already started. In order to achieve the objectives of high speed and low latency, millimeter-wave technologies will be necessarily adopted in the near future. This shift poses a set of new challenges to overcome, among them the initial access cell discovery procedure is one of the most critical.

Differently from current forth-generation (4G) long-term-evolution (LTE) technology, where the cell-search procedure is omnidirectional, in 5G systems at millimeter-wave frequencies will be necessary to adopt a directional beam forming approach to counter the high attenuation. This new process will require to scan the angular space in different directions.

In this thesis we present a new cell discovery algorithm that takes advantage of context information available through legacy networks in order to achieve a faster initial access. To test the algorithm we compute analytically the relevant probabilities and then we implement a 3rd generation partnership project (3GPP)-compliant and spatially consistent simulation environment. We compare the performance of the algorithm against other initial access algorithms and discuss the results.

# Introduction

The main objective of this thesis is to introduce and analyze a new initial access procedure for fifth-generation (5G) systems. The thesis is divided into five chapters covering the following topics:

1. We introduce the 3rd Generation Partnership Project (3GPP) new radio (NR) access standard and in particular the initial access problem. We present a literature review of related works about research on the 5G systems cell-search in with millimeter waves;

2. We thoroughly describe the 3GPP standard channel model we used to compute spatially consistent angles of arrival and departure;

3. We present the new initial access with neighbour assistance algorithm and the considered scenario. We also describe other cell-search algorithms used as comparison;

4. We display the performance analysis of all the algorithms with analytical and simulation results. The average discovery times and cumulative distribution functions (CDF) are presented for every algorithm with figures and graphs;

5. We provide final conclusions and discuss possible future developments.

# Chapter 1

# The Initial Access Problem

The 5G cellular network is expected to match the needs of users, business and industry in the next year of 2020 and beyond. 5G will enable three general aspects of the next generation mobile networks:

- enhanced mobile broadband (eMBB) providing fast connections with high throughput and high user mobility
- ultra-reliable low-latency communications (URLLC) in mission-critical applications for industry and health automation
- massive machine-type communications (mMTC) for the wide area long range and low data rate IoT use cases.

In order to fully realize all these different usage scenarios 5G will provide a great performance improvement over the existing wireless network such as:

- high throughput up to 10-20 Gbps peak and high mobility (500 km/h) to support ultra-high definition video streaming and virtual reality applications
- low communication latency, below 1 ms air interface, to support real-time mobile control
- ultra-high reliable and available (99.9999% of the time), high connectivity to support the high density of devices.

To achieve all these targets and in particular to meet the required high data rates, the 3GPP started the development of a new radio access standard known as NR [1].

The vast bandwidth available in the millimeter-wave (mmWave) spectrum makes it the best candidate for the task at hand. A mmWave is an

electromagnetic wave with a wavelength going from 10 mm to 1 mm, that corresponds to a frequency range of 30 Ghz to 300 Ghz respectively. The propagation conditions at this high frequencies are troubled by high attenuation and blockage, since mmWave signals do not penetrate most materials. To overcome this propagation loss, highly directional antenna arrays are used both at the base station (BS), or as it is called in the 3GPP standard gNB, and at the user equipment (UE) to perform beamforming (BF) and achieve a sufficient link budget.

A critical procedure in this framework is the initial access (IA) which allows a UE to establish a physical link connection with a BS. In current long-term-evolution (LTE) systems IA is performed with omnidirectional signals while BF can be used only for data transmission after a physical link is established. In 5G mmWave systems the IA procedure is constrained by strong propagation loss and regulatory power limitations therefore it is essential to exploit the antenna gains from BF even during this initial phase. On the other hand as highly directional links require fine alignment of the transmitter and receiver beams, this procedure can significantly increase the time needed to perform cell-search and access the network, contrasting with the aforementioned 5G performance target of low communication latency.

In this thesis a possible solution to reduce the time necessary to perform IA in mmWave frequencies is investigated. When entering the 5G cell, we envision that a new UE interacts with its closest neighbour UE, already connected to the BS, in order to acquire the information on the beamforming direction used to communicate with the BS and thus avoiding the need to perform a complete exhaustive search of the beam directions to find the optimal one.

## 1.1 Initial Access Overview

We now define and describe the quantities and elements that are used in the rest of this work. Our objective is to find a faster way to perform the Initial access (IA) procedure with respect to the exhaustive search. IA procedure enables a UE to acquire the proper alignment for directional transmission and reception with a Next Generation node base station (gNB). The steps required to perform the IA procedure are:

1. beam sweeping: covering a spatial area with a set of beams transmitted and received according to pre-specified intervals and directions

2. beam measurement: requires the UEs in a downlink framework (or the gNBs in an uplink one) to evaluate the quality of the received signal

3. beam determination: UEs and gNBs select the best beams according to the measurements obtained with the beam measurement procedure

4. beam reporting: information on the quality of the received beamformed signals and on the decisions in the beam determination phase is exchanged.

These procedures are periodically repeated to update the optimal transmitter and receiver beam pair over time. The details of this scheme for beam management are different in function of the architecture considered, such as SA or NSA. In a NSA configuration a BS uses an LTE cell as support for control plane management and UEs exploit multi-connectivity to maintain 4G and 5G connections active at the same time to combine the benefits of high bit rates from mmWave links and the robustness of legacy channels. In a SA configuration there is no LTE control plane to exploit.

Our research focuses on the beam sweeping phase which occupies the largest fraction of time in the IA procedure.

## 1.2 NR Overview

The technical specifications for the physical (PHY) layer are provided by the 3GPP standard. In [2], [3], [4] and [5] is explained how the waveform used in 5G NR is orthogonal frequency division multiplexing (OFDM) with a cyclic prefix, where parameters such as sub-carrier spacing and cyclic prefix duration can be adjusted to address the specific use cases. The sub-carrier spacing is $15 \times 2^n$ kHz with $n \in \mathbb{N}, n \leq 4$, a frame lasts 10 ms and is composed by 10 sub-frames of 1 ms. A slot is composed of 14 OFDM symbols and the number of slots in a sub-frame can vary between 1 to 16 depending on the sub-carrier spacing configuration used.

Beam management operations to support communications at mmWave frequencies are based on control messages which are periodically exchanged between transmitter and receiver nodes, see Fig. 1.1. The framework can be divided into downlink (DL) and uplink (UL) whether the signals are transmitted from the gNB to the UE or vice versa, respectively. Another useful division is between non-standalone (NSA) and standalone (SA) architectures according to whether the control plane is managed with the support of LTE or not, respectively.

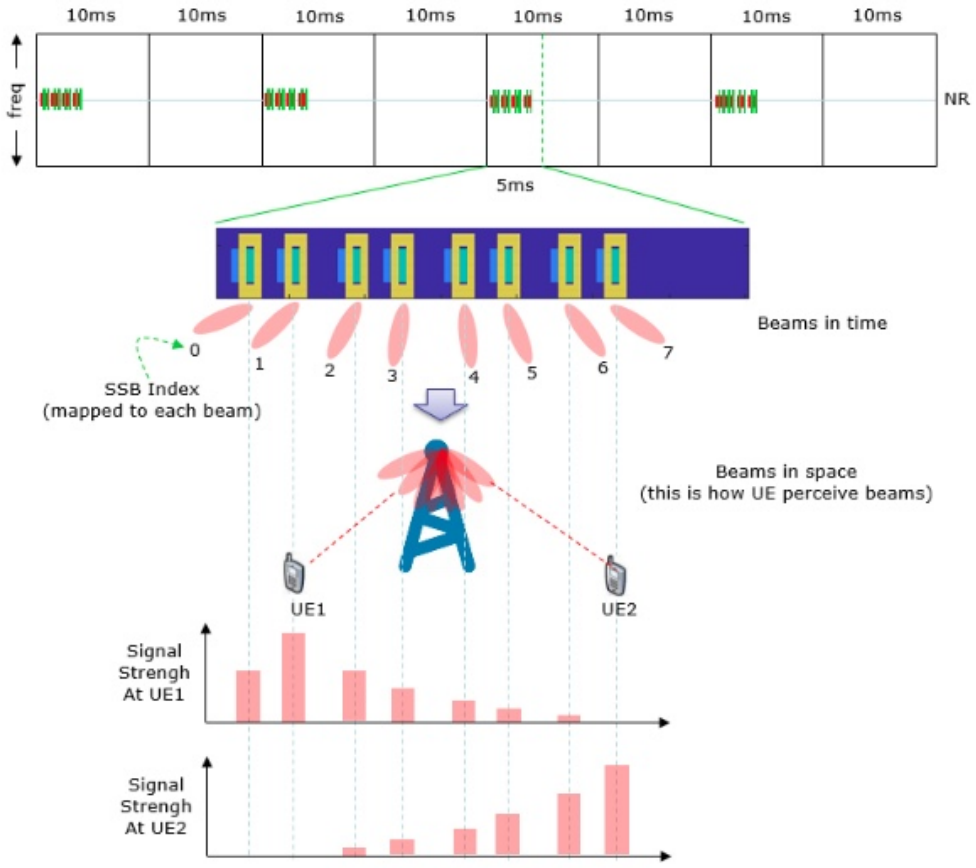


Figure 1.1: Beam management. Figure from [6].

### 1.2.1 Downlink

The DL messages defined in the 3GPP standard are synchronization signal (SS) blocks and channel state information reference signal (CSI-RS). The concept of SS block and burst is introduced for periodic synchronization signals from the gNB. The gNB periodically transmits synchronization signal (SS) burst set, where

- a SS block is composed by 4 OFDM symbols in time (240 contiguous sub-carriers in frequency) that include one primary synchronization signal (PSS), one secondary synchronization signal (SSS) and two physical broadcast channel (PBCH) that contain the demodulation reference signals (DM-RS), used to estimate the reference signal received power (RSRP) of the SS block
- SS burst consists of a finite number of SS blocks, up to 64

- SS burst set consists of a finite number of SS bursts.

In Fig. 1.2 and Fig. 1.3 we can observe the SS block structure.

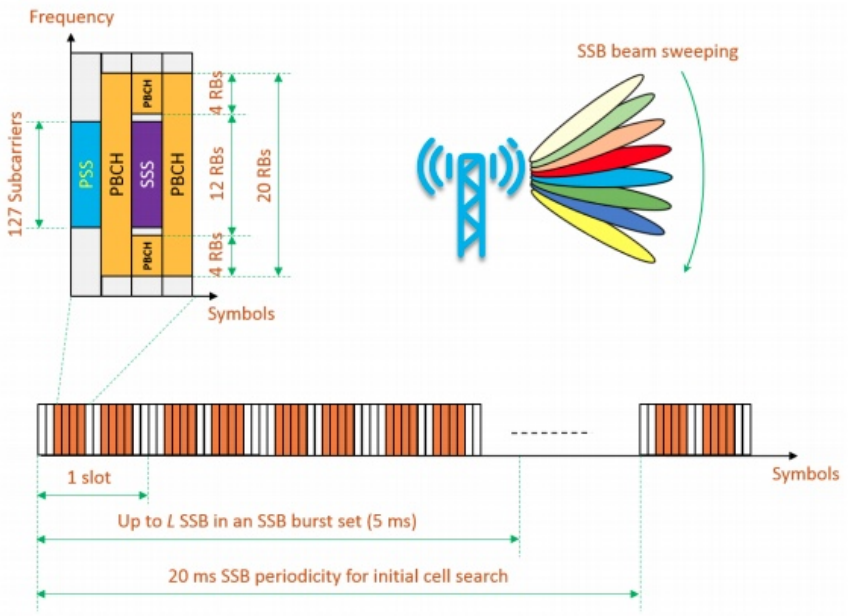


Figure 1.2: SS block structure. Figure from [7].

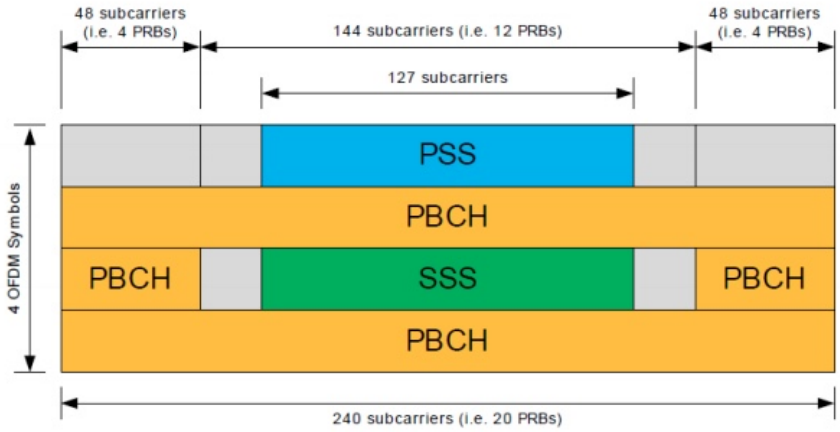


Figure 1.3: SS block detail. Figure from [8].

All the transmitted SS blocks of the set are contained on the first 5 ms of an SS burst. The maximum number of SS blocks in a SS burst is 64, that

corresponds to the maximum number of angular sectors sweeped by the BS in each period. Each of these SS blocks has a unique number called SS block index and is transmitted by the BS with a specific beam-former radiating in a certain direction. The UE located inside the gNB cell measures the signal strength of each SS block it detects for a certain period of time. From the measurements the UE can identify the SS block index corresponding to the strongest received signal, this is the best beam for the UE that then proceeds to notify on the physical random access channel (PRACH) the SS block index to the gNB. As a DL only signal, the CSI-RS that the UE receives is used to estimate the channel and report channel quality information back to the BS.

As a DL only signal, the CSI-RS the UE receives is used to estimate the channel and report channel quality information back to the BS. The CSI-RS can be 1,2 or 4 OFDM symbols long and the CSI measurements are used to derive the signal quality of the various beams.

### 1.2.2 Uplink

Beam management while in idle mode uses PSS, SSS and PBCH DM-RS to perform IA whereas in connected mode uses CSI-RS in DL and Sounding Reference Signal (SRS) in uplink to perform tracking. As a UL only signal, the SRS is transmitted by the UE to help the gNB obtain the CSI for each user and to monitor the uplink channel quality.

For our purposes we assume a static environment, where user positions are fixed. The setting consists of a circular 5G cell, with radius of $l$ meters and with the BS positioned in the center of the cell. Inside the cell we position two UEs A and B. A is the new UE that has to perform the IA procedure, while B is the closest UE to A that is already linked to the BS. The BS and UEs will transmit symbols with a carrier frequency $f_c$ and the angular space is divided in a number of sectors $s$. We indicate with $d$ the distance in meters between the gNB and a UE.

### 1.2.3 Standalone-Downlink (SA-DL) Scheme

- Beam sweeping: the process is carried out with an exhaustive search during which the BS and UE transmit and receive, respectively, synchronization and reference signals using a predefined sequence of directions that spans the whole angular space.

- Beam measurements: the measurements for IA are based on the SS blocks while for the tracking both SS bursts and CSI-RS are used.

- Beam determination: the UE selects the best beam among all those above a predefined threshold. The corresponding angular sector will be used for the subsequent transmissions.

- Beam reporting: during the IA phase, after beam determination, the UE has to wait for the BS to schedule a Random Access Channel (RACH) opportunity towards the best direction just determined in order to perform random access and to inform the BS of the optimal direction where to steer its beam. For each SS block the BS opens one or more RACH opportunities with a certain time, frequency and direction, so that the UE knows when to transmit the RACH preamble. This process can require an additional complete directional scan of the BS, increasing the total time it takes to access the network. During the tracking phase, in connected mode, the UE can provide feedback by using the control channel already established.

### 1.2.4 Non-Standalone-Downlink (NSA-DL) Scheme

In this case the first three steps of the procedure are the same as in the SA-DL case. In the beam reporting phase the presence of the LTE connection enables the UE to report the optimal beam direction to the BS without waiting for an additional beam sweep. Routing the signals from the UE to the BS via LTE connection allows to immediately schedule a RACH opportunity in the selected direction.

### 1.2.5 Non-Standalone-Uplink (NSA-UL) Scheme

This framework is based on the channel quality of the UL signals with the support of a central LTE evolved Node Base (eNB). In this case each UE transmits SRS signals continuosly sweeping the angular space, while each BS scans and monitors all its angular directions building a report table based on channel quality of each direction. Once the report table of each BS has been filled for every UE it is then sent to the LTE eNB that computes the best match between the beams of UEs and BSs. The eNB then proceeds to inform the UEs through LTE link which BS to connect to and also the optimal direction where to steer its beam. Finally the eNB notifies the BS through a backhaul high capacity link about the optimal direction in which to steer the beam for serving the UE.

## 1.3 Literature Review

Research on the IA procedure for 5G systems in mmWave frequency range has been active at least since 2014 [9]. The main areas of research evolve around two distinct types of approach for IA: autonomous search and context-information (CI) search. Autonomous search utilizes only signals exchanged between the entering UE and the BS without utilizing any aid from external communication, other devices or any localization methods [2]. On the other hand CI-based approaches can exploit different kind of useful information in order to make the IA procedure faster. Another useful division to keep in consideration is between non standalone (NSA) and standalone (SA) solutions.

In [10] a learning approach is investigated, where successful beamforming configurations are stored and used to drive future user detection. The algorithm takes into consideration also the possibility to avoid obstacles in the path by using reflected rays. In [11] a cell discovery procedure that exploits user position information and a non standalone (NSA) configuration is investigated. The NSA scenario provides the simultaneous presence of both LTE and 5G networks where the control plane is linked to LTE base stations while user plane data is exchanged with mmWave BS. In [12] a CI method is proposed where the best directions to explore for incoming UEs are found using machine learning techniques on information about past access attempts.

In [13] a comparative analysis is given for various autonomous search IA techniques such as exhaustive and iterative search. The exhaustive search consists on a predefined sequential beam search that spans the whole angular space while the iterative search performs a two-stage scan of the angular space: first with a small number of macro beams that cover all the angular space, then with narrow beams covering only the angular space of the best beam found during the first stage. Overall the optimal strategy depends on the target SNR regime, anyhow the exhaustive search has a lower misdetection probability (PMD) and total delay in many situations. An extension of this work is given in [14], where the investigation is extended to CI based NSA algorithms in which UEs are informed about the location of surrounding BSs through an LTE link. In [15] a NSA solution is investigated, where the CI regarding the BS geolocation is available to the UEs via a LTE link. In particular the authors show that with this technique the performance of an analog beamformer at the UE can be greatly improved avoiding the need to scan all the angular space.

In [16], [17], and [18] a thorough review of the design and dimensioning of beam management frameworks and parameters is given. In particular the analysis covers uplink (UL) and downlink (DL) frameworks, SA and NSA

architectures and different beamforming architectures: analog, hybrid and digital. The authors used a realistic mmWave channel model to simulate the various scenarios and in general the results proved that the optimal parameter choices to achieve fast IA depend on the specific environment.

In [19], and [20] a CI approach is studied where the statistical information about the time and direction of arrival in the cell of the UEs are stored and used to narrow the search space of the beam to perform IA. The authors show that by searching more often in the most probable sectors in which to find UEs, the discovery time can be greatly reduced with respect to autonomous search methods that do not exploit user statistics.

In [9], [21], [22], and [23] the authors propose a cell discovery procedure where a BS periodically transmits synchronization signal in random directions and the UEs use a generalized likelihood ratio test (GLRT) to search for the signals. Moreover different design options for the UEs and the signals are evaluated, in particular using omnidirectional versus directional antennas and analog versus digital beamforming. The result shows that omnidirectional transmission from the BS outperforms random directional scanning and performing digital beamforming at the UE, where the UE can search in all directions at once, makes the IA procedure significantly faster than using analog beamforming that permits the UE to scan only in one direction at a time.

In [24] the authors propose a SA, non CI, sequential beamforming strategy to perform IA while minimizing the average miss-discovery probability of UEs. The strategy proposed uses a pre-designed beamforming codebook for transmitting the reference signals. The results show that this method is much more effective in detecting UEs, also in the presence of blockage, with respect to random beamforming.

In [25] four different SA, non CI, IA protocols are studied. The protocols for BS and UE used to determine the beamforming directions are:

- exhaustive search, BS and UE sweep through all possible directions during cell-search (CS) and during random access (RA) UE transmits in the direction found during CS phase
- fast RA, CS is the same as in exhaustive search, during RA the BS receives omni-directionally
- fast CS, same as exhaustive search but during CS the BS utilizes a wide beam
- omni RX, during CS the UE receives omni-directionally and the BS receives omni-directionally during RA

After deriving several performance metrics the authors show that the best trade-off between IA delay and user-perceived DL throughput is achieved with fast CS protocol.

In [26] a NSA, CI solution based on feeding location information to a support vector machine (SVM) is studied to speed up the IA procedure. The results show that with enough previous location information the algorithm can reduce the IA delay.

# Chapter 2

# 3GPP Channel Model

In this chapter we describe the 3GPP channel model we used to compute spatially consistent angles of arrival (AoA). First we describe the procedure to compute LOS/NLOS state, then we detail the AoA generation procedure in three steps: LOS AoA, cluster AoA and final AoA. We also describe how to obtain spatial consistency by correlation of small scale parameters.

The channel model we use is a spatially-consistent version of the Urban Micro (UMi) outdoor to outdoor (O2O) model, defined in the 3GPP TR 38.901 [27] technical report. The most relevant scenario for our initial access problem is the outdoor street canyon, since we are dealing with millimeter waves. The effects of high path loss, shadowing, and blockage are likely to limit the adoption of mmWave mainly to open urban environments like city centers, squares, and parks. The model is valid for millimeter wave frequencies up to 100 GHz. The UMi (street canyon, open area) scenario is intended to capture real-life situations such as a city or a station square, as can be seen in Fig. 2.1.

The cell layout is a square grid, of side length $l$, with one base station (BS) located at the center and a number of user equipments (UEs). In the 3GPP standard the number of sectors that divide the angular space for cell-search and beam sweeping procedure is frequency dependent as specified in [3] and is equal to the number of synchronization signal (SS) blocks transmitted in a SS burst. The maximum number of predefined directions (beams / SS blocks, see Fig. 2.2) in the SS burst set is 64 for carrier frequencies larger than 6 GHz and subcarrier spacing of 120 or 240 kHz.

In Fig. 2.3 the outdoor distance $d_{2D}$ between BS and UE is defined as the distance between the base of the two devices.

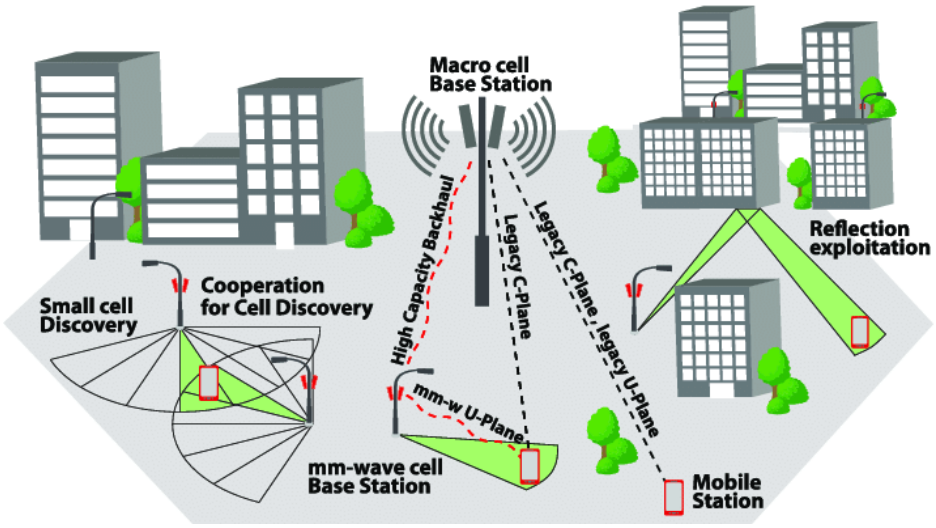


Figure 2.1: mmWave UMi scenario. Figure from [11].

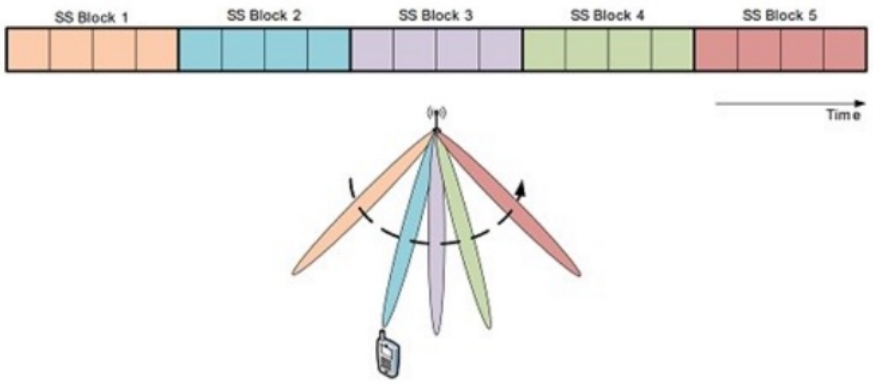


Figure 2.2: Beam sweeping sectors. Figure from [8].

## 2.1 Line Of Sight Probability

The line-of-sight probabilities are computed for every point of the grid with the equation provided in Table 7.4.2-1 of [27]:

The radio channel realizations are created using the parameters listed in Table 7.5-1 of [27] and the spatial consistency procedure described in section 7.6.3 of [27]. We are interested in the correlation of the angles of arrival (AoA) and departure (AoD) of the two UEs. First we define some useful parameters reported in Table 2.1.

Following the 3GPP procedure [27] for a spatially consistent simulation

Table 2.1: Parameters of UMi channel model.

| **Parameter** | **Notation** | **Value** |
|---|---|---|
| Carrier frequency | $f_c$ | $[0.5, 100]$ GHz |
| Line of sight (LOS) AoA | $\phi_{\text{LOS,AoA}}$ | $[0°, 360°]$ deg |
| Line of sight (LOS) AoD | $\phi_{\text{LOS,AoD}}$ | $[0°, 360°]$ deg |
| Number of clusters | $N$ | $[1, 19]$ |
| Number of rays | $M$ | $[1, 20]$ |
| Correlation distance | $\Delta_{\text{Corr}}$ | $\begin{cases} 12 \text{ m} & \text{LOS} \\ 15 \text{ m} & \text{NLOS} \end{cases}$ |
| LOS/NLOS correlation distance | $\text{C}_{\text{LOS/NLOS}}$ | 50 m |
| Cluster azimuth spread of arrival angles (ASA) | $c_{\text{ASA}}$ | $\begin{cases} 17° & \text{LOS} \\ 22° & \text{NLOS} \end{cases}$ |
| Cluster azimuth spread of departure angles (ASD) | $c_{\text{ASD}}$ | $\begin{cases} 3° & \text{LOS} \\ 10° & \text{NLOS} \end{cases}$ |
| Ray offset angles within a cluster | $\alpha_m$ | see Table 2.2 |
| Cell side length | $l$ | 300 m |
| BS spatial coordinates | $[x_{\text{BS}}, y_{\text{BS}}]$ | $[\frac{l}{2}, \frac{l}{2}]$ |
| i-th UE spatial coordinates | $[x_i, y_i]$ | $[0, l] \times [0, l]$ |

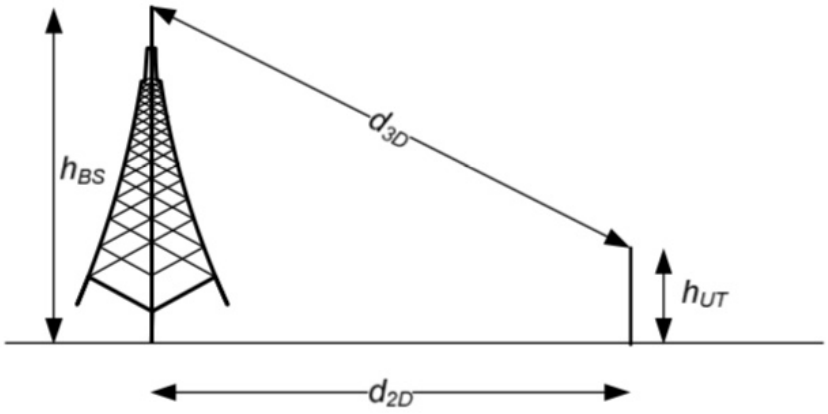


Figure 2.3: Definition of outdoor $d_{2D}$. Figure from [27].

we describe the model used to simulate AoA and AoD in both LOS and NLOS conditions. The scenario taken into consideration includes one BS located in the center of the cell and two UEs. This simulation concerns only the generation of AoA and AoD values, therefore every unnecessary step contained in the fast fading model has been skipped. The simulation is able to compute for every point of the cell the AoA and AoD value for any number of clusters $N$ and $M$ rays ($1 \leq M \leq 20$).

First we generate a 2-D meshgrid where each point represents a sampled value of the probability of being in LOS condition. Sampled points are separated by a distance larger than the correlation distance for LOS/N-LOS state: $\mathrm{C_{LOS/NLOS}}$. We compute the distance between the BS, placed in position $(x_{\mathrm{BS}}, y_{\mathrm{BS}})$, and a generic point $(x, y)$ of the grid as:

$$d_{2D}(x, y) = \sqrt{|x_{\mathrm{BS}} - x|^2 + |y_{\mathrm{BS}} - y|^2}. \tag{2.1}$$

The probability of being in LOS condition is

$$\mathrm{P_{LOS}}(x, y) = \begin{cases} 1 & \text{if } d_{2D} \leq 18 \text{ m} \\ \frac{18}{d_{2D}} + (1 - \frac{18}{d_{2D}})e^{-\frac{d_{2D}}{36}} & \text{if } d_{2D} > 18 \text{ m} \end{cases}. \tag{2.2}$$

Then the probability of being in LOS condition for points not on the grid is obtained by interpolation using the MATLAB function *interp2*. An example of interpolated probability is given in Fig. 2.4. The interpolated probability (2.2), see Fig.2.5, is then intersected with a plane at height 0.5 in order to discriminate between LOS and NLOS areas and visualize the contours inside the grid as in the example of Fig. 2.6.

Table 2.2: Ray offset angles within a cluster.

| **Ray number** $m$ | **Offset angle** $\alpha_m$ |
|---|---|
| $1, 2$ | $\pm$ 0.0447 |
| $3, 4$ | $\pm$ 0.1413 |
| $5, 6$ | $\pm$ 0.2492 |
| $7, 8$ | $\pm$ 0.3715 |
| $9, 10$ | $\pm$ 0.5129 |
| $11, 12$ | $\pm$ 0.6797 |
| $13, 14$ | $\pm$ 0.8844 |
| $15, 16$ | $\pm$ 1.1481 |
| $17, 18$ | $\pm$ 1.5195 |
| $19, 20$ | $\pm$ 2.1551 |

## 2.2 Angle Of Arrival and Departure Generation

The procedure hereafter described is the same for AoA and AoD generation, to avoid repetition we will only refer to AoA, but all the discussion remains valid for AoD.

The computation of the AoA follows the procedure B specified in Section 7.6.3.2 of [27] and here is divided into three steps: LOS AoA, cluster AoA and final AoA.

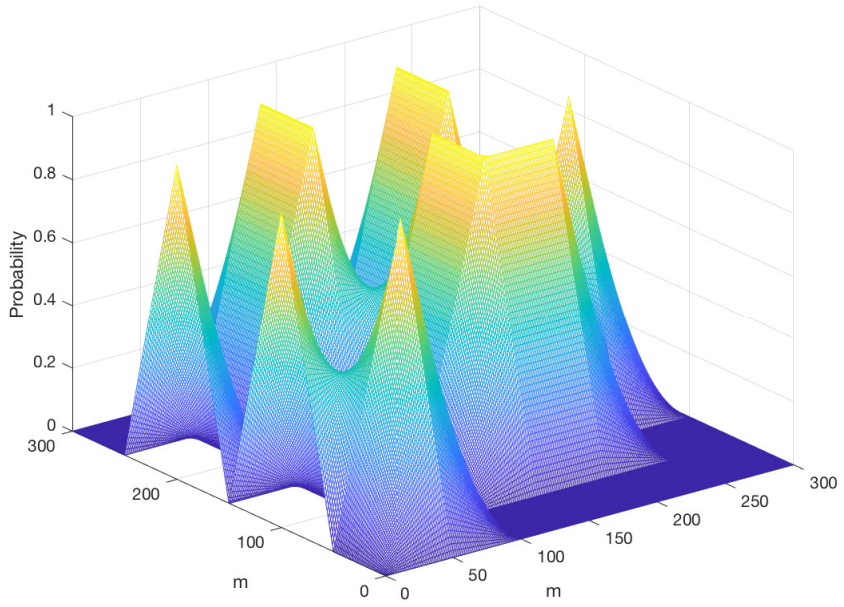


Figure 2.4: LOS Probability example on a $300 \times 300$ meters UMi grid.

### 2.2.1 LOS Angle Of Arrival

For each point in the grid, either in LOS or NLOS, we compute the angle formed with respect to the BS

$$\phi_{\text{LOS,AoA}}(x,y) = \begin{cases} \arctan(\frac{y-y_{\text{BS}}}{x-x_{\text{BS}}}) & \text{if } x > x_{\text{BS}} \text{ and } y > y_{\text{BS}} \\ \arctan(\frac{y-y_{\text{BS}}}{x-x_{\text{BS}}}) + 360° & \text{if } x > x_{\text{BS}} \text{ and } y < y_{\text{BS}} \\ \arctan(\frac{y-y_{\text{BS}}}{x-x_{\text{BS}}}) + 180° & \text{if } x < x_{\text{BS}} \\ +90° & \text{if } x = x_{\text{BS}} \text{ and } y > y_{\text{BS}} \\ -90° & \text{if } x = x_{\text{BS}} \text{ and } y < y_{\text{BS}} \\ 0° & \text{if } x = x_{\text{BS}} \text{ and } y = y_{\text{BS}}. \end{cases} \tag{2.3}$$

We used the MATLAB command *atan2d* adjusting it so to obtain an output angle in $[0, 360]$ degrees. An example of the result can be seen in fig 2.7. The *atan2d(Y, X)* command computes the four-quadrant inverse tangent and returns values in $[-180°, 180°]$ degrees based on the values of $y$ and $x$ as shown in Fig. 2.8.

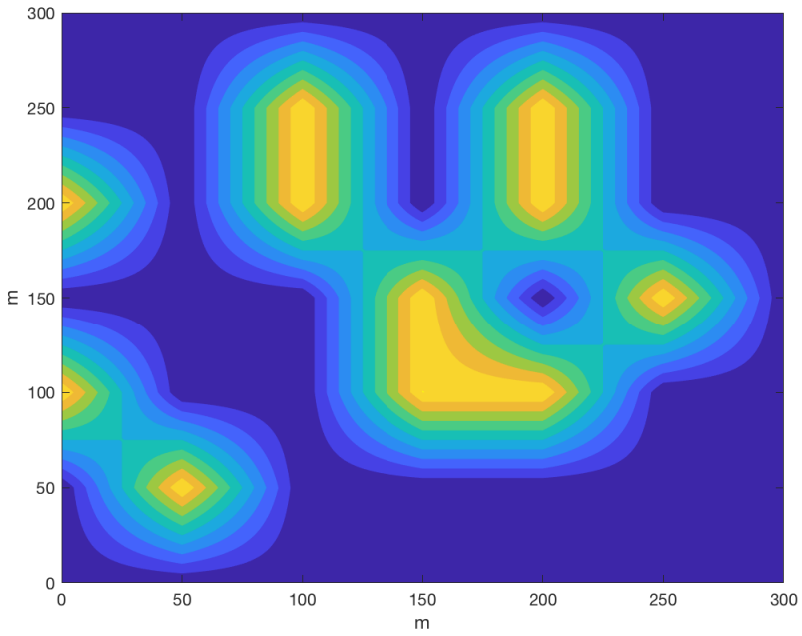


Figure 2.5: LOS Area contour example before plane intersection.

### 2.2.2 Cluster Angles Of Arrival

The mean and standard deviation of the azimuth spread of arrival angles (ASA) and azimuth spread of departure angles (ASD), as a function of the carrier frequency $f_c$, are computed as:

$$\mu_{\text{lgASA}} = \begin{cases} -0.08\log_{10}(1+f_c) + 1.73 & \text{if LOS} \\ -0.08\log_{10}(1+f_c) + 1.81 & \text{if NLOS,} \end{cases} \tag{2.4}$$

$$\sigma_{\text{lgASA}} = \begin{cases} 0.014\log_{10}(1+f_c) + 0.28 & \text{if LOS} \\ 0.05\log_{10}(1+f_c) + 0.3 & \text{if NLOS,} \end{cases} \tag{2.5}$$

$$\mu_{\text{lgASD}} = \begin{cases} -0.05\log_{10}(1+f_c) + 1.21 & \text{if LOS} \\ -0.23\log_{10}(1+f_c) + 1.53 & \text{if NLOS,} \end{cases} \tag{2.6}$$

$$\sigma_{\text{lgASD}} = \begin{cases} 0.41 & \text{if LOS} \\ 0.11\log_{10}(1+f_c) + 0.33 & \text{if NLOS,} \end{cases} \tag{2.7}$$

where $f_c$ is the carrier frequency expressed in gigahertz and the notation for mean and standard deviation is used for logarithmized parameters: $\mu_{\text{lgX}} = \text{mean}\{\log_{10}(X)\}$ and $\sigma_{\text{lgX}} = \text{std}\{\log_{10}(X)\}$.

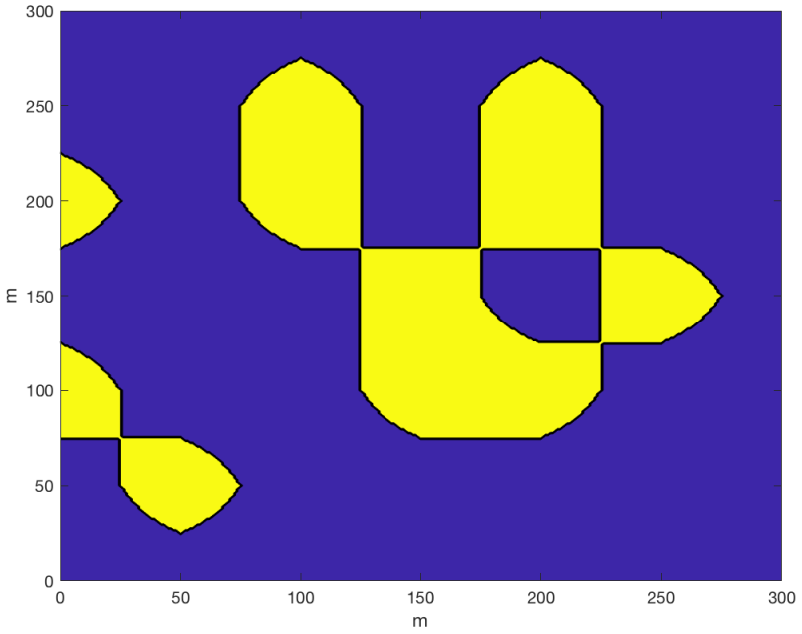


Figure 2.6: LOS Area contour example after plane intersection.

We generate $N$ arrival and departure angles for azimuth component of each cluster $n = 1, \ldots, N$, for every point in the grid as

$$\text{ASA} = min(2 \cdot 10^{\mu_{\text{lgASA}} + \sigma_{\text{lgASA}}}, 104^\circ) \tag{2.8}$$

$$\phi'_{n,\text{AoA}} \sim \text{ASA} \cdot u_n \quad \text{with} \quad u_n \in \mathcal{U}(-1, 1), \tag{2.9}$$

where $\mathcal{U}$ is the uniform distribution and in the LOS case, for the first cluster, we set $\phi'_{1,\text{AoA}} = 0$.

### 2.2.3 Final Angle Of Arrival

Now we have computed for each spatial point the LOS angle, $\phi_{\text{LOS,AoA}}$, and the angle of the azimuth component for each cluster $\phi'_{n,\text{AoA}}$. At each point is also added the cluster spread of arrival angles:

$$c_{ASA} = \begin{cases} 17 & \text{if LOS} \\ 22 & \text{if NLOS} \end{cases} \tag{2.10}$$

multiplied by the ray offset angle $\alpha_m$ with values taken from Table 7.5-3 in [27] and reported in Table 2.2. Finally the angle of arrival of every cluster $n$

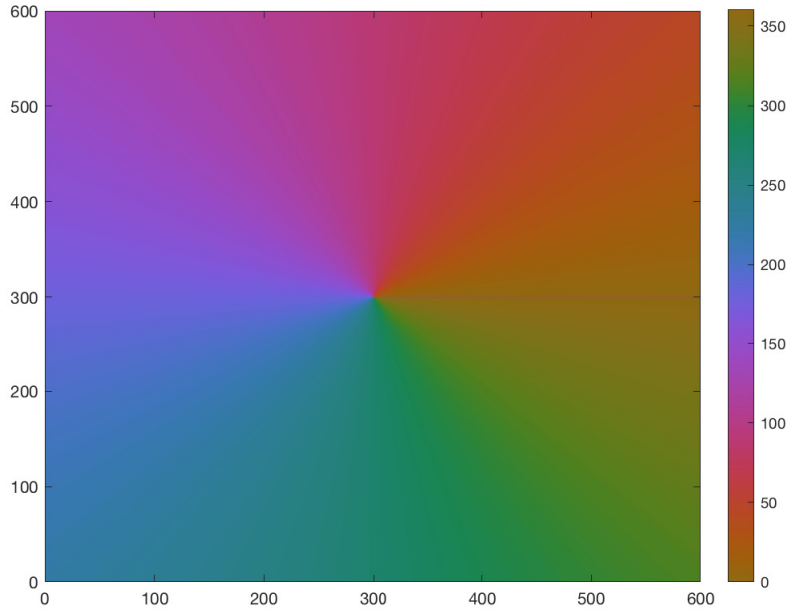


Figure 2.7: $\phi_{\mathrm{LOS,AoA}}$

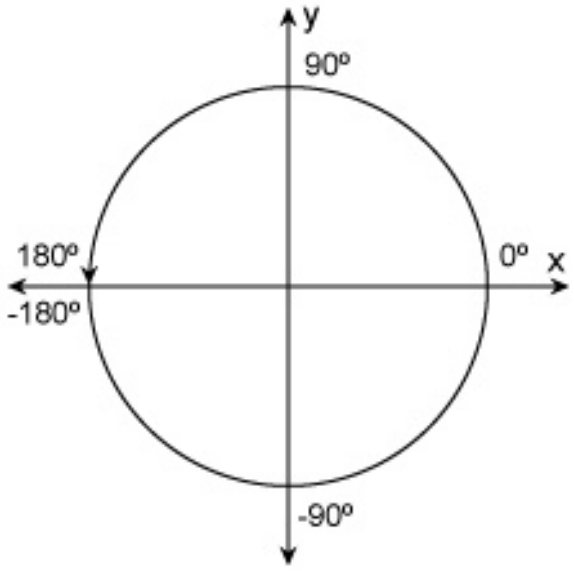


Figure 2.8: Four-quadrant inverse tangent.

and every ray $m$ in each point of the grid is computed as:

$$\phi_{n,m,\text{AoA}} = \phi'_{n,\text{AoA}} + \phi_{\text{LOS,AoA}} + c_{\text{ASA}}\alpha_m. \tag{2.11}$$

The generation of AoD ($\phi_{n,m,\text{AoD}}$) follows a procedure similar to AoA as described above.

An example of a single realization of the first ray of the first cluster can be seen in Fig. 2.9, in Fig. 2.10 the sum of the three angular components for the first ray of the first cluster ($n = 1$ and $m = 1$), while in Fig. 2.11 is a polar plot of the angles of arrival in a selected point with 3 clusters, each cluster composed of 4 rays.

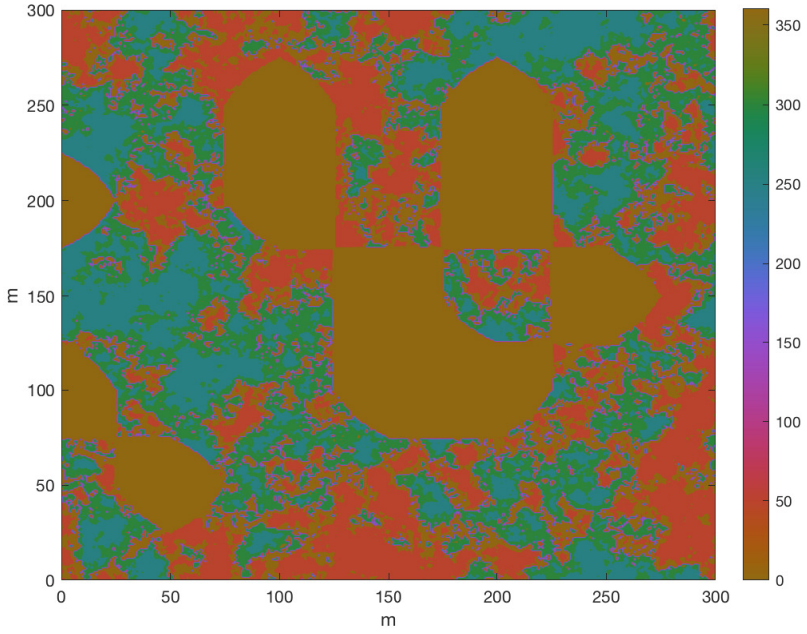


Figure 2.9: $\phi'_{n,\text{AoA}}$.

### 2.2.4 Spatial Consistency Procedure

Now we explain in more detail how we actually extract values from (2.9). Since we want the channel to be spatially consistent we follow the procedure illustrated in [28], see Fig. 2.12. There are two main steps: first we generate independent Gaussian random variables $Y$, these independent variables are then filtered in order to obtain correlated Gaussian random variables $V$.

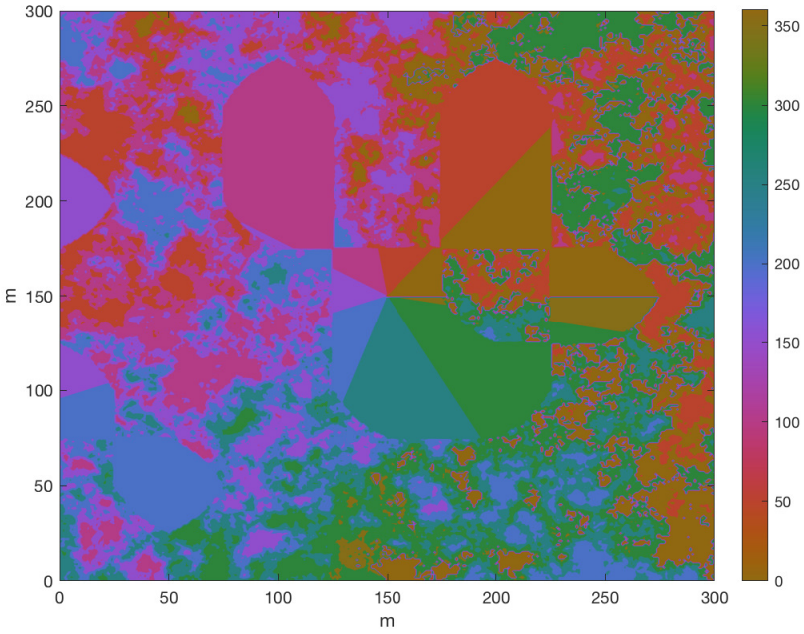


Figure 2.10: $\phi_{AoA} = \phi'_{n,m,\text{AoA}} + \phi_{\text{LOS,AoA}} + c_{\text{ASA}}\alpha_m$.

Then we perform a non linear transformation to $V$ in order to generate the prescribed uniform random variable $Z$ with desired correlation.

### Linear Transformation

First we generate a random Gaussian value for every point of the grid, extracted from independent normal Gaussian random variables $Y$. Then we impose an exponential correlation $\rho$ between different spatial points of the grid with distance $d$ and correlation distance $\Delta_{\text{Corr}}$ (see Table 7.6.3.1-2 in [27])

$$\rho(d) = e^{-\frac{d}{\Delta_{\text{Corr}}}}. \tag{2.12}$$

This is achieved by linear transformation, i.e. by linear filtering the independent Gaussian values with a two dimensional FIR filter, with impulse response (2.12), see Fig. 2.13.

The actual filtering is performed in the frequency domain by multiplying the Fourier transform of the independent Gaussian values with the square root of the Fourier transform of the filter appropriately normalized.

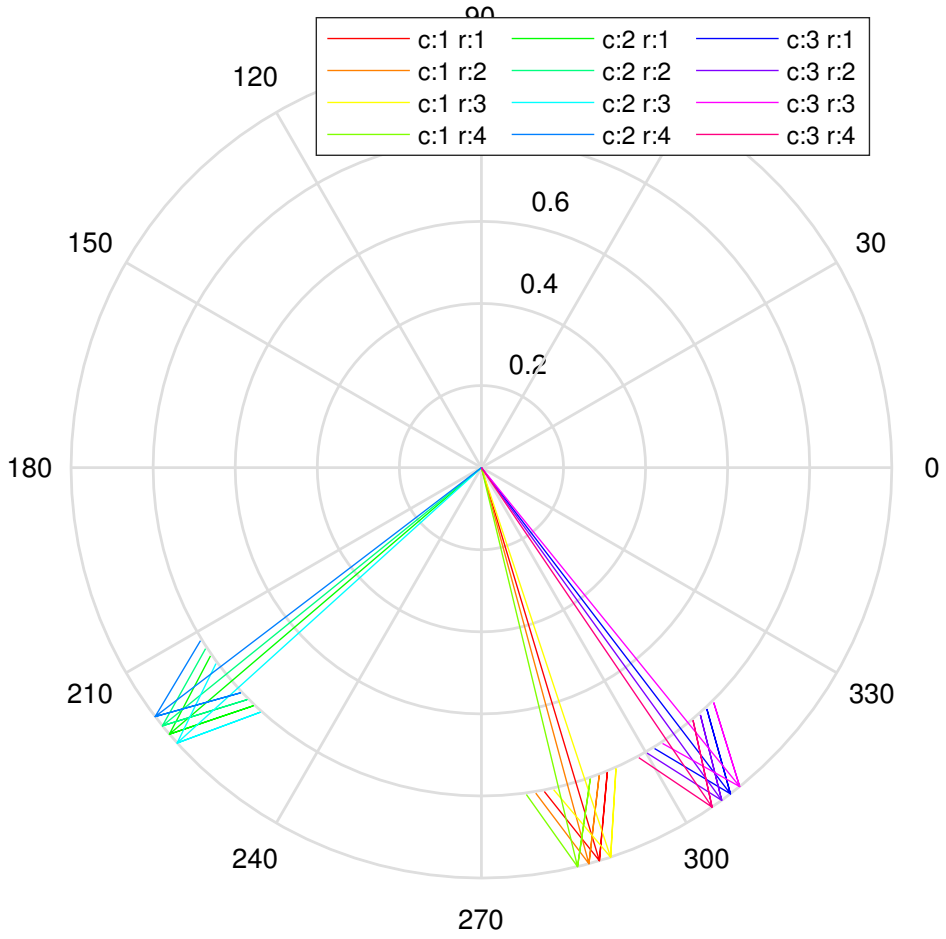


Figure 2.11: Polar plot.

### Non Linear Transformation

Now from the correlated normal Gaussian random variables $V$ we obtain the correlated uniform random variables $Z$ by applying a non linear transformation. The random component $u_n$ of (2.9) has a uniform distribution $z \sim \mathcal{U}(-1, 1)$. We recall the inverse of the cdf of the uniform distribution

$$F_Z^{-1}(x) = 2x - 1, \tag{2.13}$$

we can obtain $z$ using the following result from [28]

$$z = F_Z^{-1}\left(F_V(v)\right) = \operatorname{erf}\left(\frac{v}{\sigma\sqrt{2}}\right) \tag{2.14}$$

where $\operatorname{erf}(\cdot)$ is the error function. This procedure allows us to achieve the desired correlation in the uniformly distributed cluster AoA (2.9).

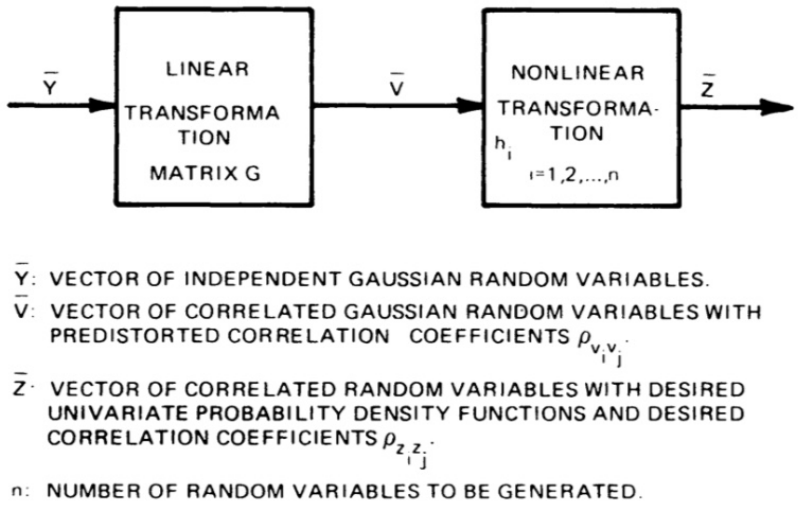


Figure 2.12: Method for generating correlated uniform random variables. Figure from [28].

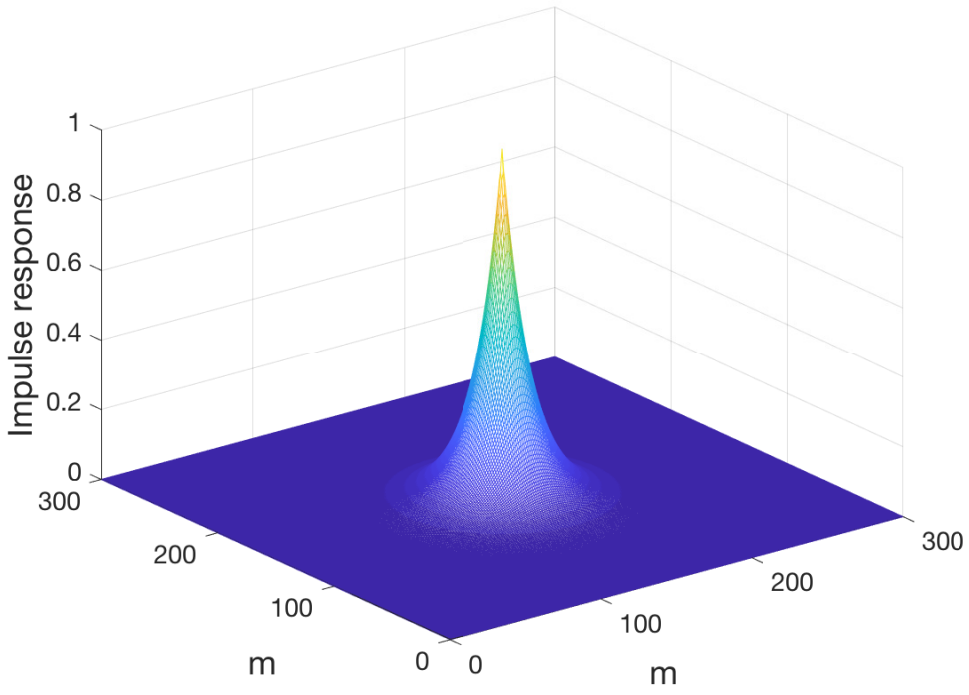


Figure 2.13: FIR filter impulse response.

# Chapter 3

# Initial Access With Neighbour Assistance

In this chapter we describe the novel idea of [29] on how to solve the problem of initial access (IA). We outline the problem of IA and the scenario considered and then explain the proposed solution with its algorithm.

## 3.1 Problem And Scenario Description

In the previous chapter we delved into the 3GPP standard. Surely the adoption of mm-wave communications will be a key enabler to reach 5G bandwidth, speed and latency goals. On the other hand many network functions will be affected by the physical layer properties of mm-wave. Among the various critical network functions our goal is to find a faster solution to the IA cell-search problem by exploiting context information.

We assume that context information like UEs and BS coordinates, distances, and active sector are available to every device in the 5G cell through legacy LTE macro cells.

We consider a mm-wave link between a base station (BS) and a user equipment (UE) where both devices are equipped with multiple antennas. The high frequency mm-waves suffer a strong attenuation so, in order to establish a working communication between the devices, both the BS and the UE must use beamforming to ensure that an adequate amount of power is transferred from the transmitter to the receiver. In the proposal [29] the aim is to find a direction of transmission that carries enough power to establish a useful connection. In this way we are free from the need to scan the entire angular space, this enable us to achieve a faster IA procedure. In our simulations we always assume that for every point in the cell one and

only one sector exceeds the power threshold sufficient to establish a working connection. We also assume that the spatial orientation of the devices is taken into account before performing the cell-search procedure so that every sector has the same direction for every device in the cell, whatever its rotation on the three axis.

The solution to reduce the time needed to perform IA and identify the best direction of transmission exploits the knowledge of the channel status, in particular the active sector, of nearby UEs already connected to the 5G BS.

The scenario we used to test our idea provides a single cell with a BS located at the center and a number of UEs. Both UEs and BS are equipped with multiple antennas so that they are able to focus their beam while transmitting or receiving signals. A new UE, called $UE_1$, enters into the cell and starts the search for the direction of transmission to the BS and also the BS must find the direction of transmission to $UE_1$. We assume that inside the cell at least another UE is present, called $UE_2$, that has already performed the IA procedure with the BS. For our study we also assume that the context information like the active beam sector used by $UE_2$ and the coordinates of $UE_2$ and BS are made available to $UE_1$ through a legacy network, like LTE. In Fig. 3.1 we outline a general scenario representation with BS, UEs, LOS components, active sectors and rays.

## 3.2 Algorithm Description

In this section we outline the algorithm of [29], nearest neighbour (NN) sector search, as a possible solution to achieve faster IA times. Along with this algorithm we also present here other two different algorithms: LOS sector search and random sector search. We implemented these two different approaches to solve the problem at hand in order to have a valid comparison for the NN algorithm. After performing some simulations we devised some new algorithms that combines NN and LOS approach. We thus provide a description of the sub-optimal, threshold based, NN-LOS mixed sector search and of the optimal sector search algorithm.

### 3.2.1 Nearest Neighbour Sector Search

The nearest neighbour sector search provides that a new user interacts with its neighbours in order to obtain the correct direction where to steer its beam to reach the BS. We suppose that the BS and the UEs have access to context information such as the position of all the devices involved and the beam

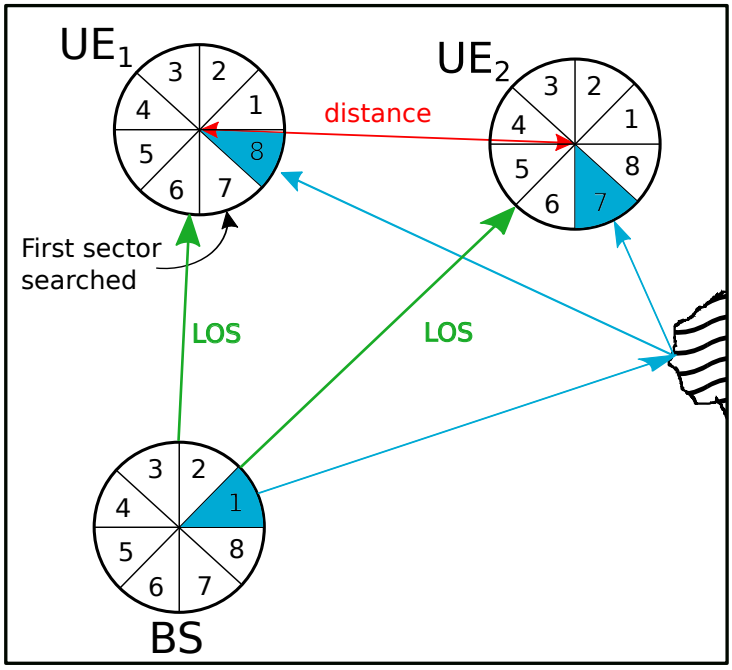


Figure 3.1: Scenario representation.

direction used by the BS to communicate with neighbour UEs. When a new UE, indicated with $UE_1$, enters the 5G cell, the BS is notified of $UE_1$ position from the LTE cell and can then determine the UE nearest to $UE_1$ already connected to the cell, called $UE_2$. Moreover, when $UE_1$ enters the 5G cell it is notified from the cell about the positions of its neighbours, $UE_2$ and its active sector. At this point both BS and $UE_1$ will start the cell-search algorithm, first by steering their antennas in the direction used for the neighbouring $UE_2$ and then exploring the angular space in an alternating *zig-zag* fashion until they measure a power level $P_k$ above a working threshold $th$.

The sequence of visited sectors is shown in Table 3.1, where in the last row 0 corresponds to the same sector used by $UE_2$, 1 is the adjacent counter-clockwise sector and $-1$ is the adjacent clockwise sector.

In order to determine the nearest neighbor $UE_2$, it is possible to proceed with one of the following methods:

- assessing the received power when UEs are transmitting with omni-directional power

- using an omni-directional transmission by the nearby UEs on another band

**Algorithm 1:** Nearest Neighbour Sector Search.

**Input:** active sector of $UE_2$
**Output:** active sector of $UE_1$
**begin**
  $k \longleftarrow$ active sector of $UE_2$;
  $i \longleftarrow 1$;
  **while** $P_k < th$ **do**
    $k \longleftarrow k + \frac{1}{4}(-1)^i(2i + (-1)^i - 1)$;
    $i \longleftarrow i + 1$;
  **end**
  **return** $k$
**end**

Table 3.1: Sector order of visit.

| **i** | 1 | 2 | 3 | 4 | 5 | 6 | 7 | 8 | 9 | 10 | ... |
|---|---|---|---|---|---|---|---|---|---|---|---|
| **f(i)** | 0 | 1 | −1 | 2 | −2 | 3 | −3 | 4 | −4 | 5 | ... |

- using the geographical positions of UEs shared by higher layer procedures, possibly through the LTE eNB.

The BS can identify $UE_2$ by

- receiving this information from either $UE_1$ or $UE_2$ through an existing communication channel
- using the geographical positions of the UEs shared by higher layer procedures.

The acquisition by the BS of the selected beamforming angle used to transmit to $UE_2$ is immediate since the index is already used by the BS itself. $UE_1$ can retrieve the beamforming angle from $UE_2$ using one of these methods:

- require that all the UEs of the cell transmit in broadcast on each sector a message containing the sector of transmission used to communicate with the BS
- require $UE_2$, upon request from $UE_1$, to transmit on each sector a message containing the sector of transmission.

In Fig. 3.2 we outline a scenario representation of the NN sector search.

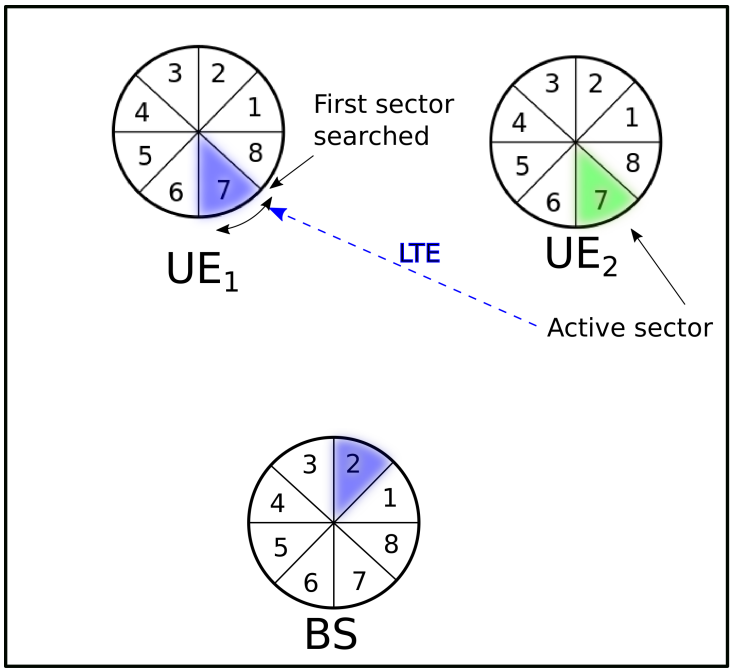


Figure 3.2: Nearest Neighbour Sector Search.

### 3.2.2 LOS Sector Search

This algorithm is based on [11]. The proposed algorithm, here called *LOS sector search*, exploits context information about the position of BS and UE made available to the devices in play through legacy technologies, like LTE. The LOS sector search algorithm provides that a new user entering the 5G cell is handed the GPS coordinates of the BS by the LTE network. Assuming the device knows its own GPS coordinates it can now compute the line of sight direction where to steer its antennas in order to find a communication path with the BS. The same procedure can be applied to the BS, where the BS receives the incoming UE coordinates from the LTE cell. Assuming the BS knows its own GPS coordinates it can thus compute the line of sight direction where to point its antennas in otder to find a connection with the new UE.

Where $\phi_{\text{LOS,AoA}}$ is computed as in (2.3). This algorithm does not require interaction with neighbouring UEs but requires the knowledge of precise position of the new UE and the BS. The first sector searched by the algorithm is the one corresponding to the LOS between the two devices, then it proceeds to scan the angular space in an alternating fashion until it finds a power level $P_k$ greater than a predefined threshold $th$. In Fig. 3.3 we outlined a scenario representation for the LOS sector search algorithm.

**Algorithm 2:** LOS Sector Search.

**Input:** coordinates of BS
**Output:** active sector of $UE_1$
**begin**
  $(x_{BS}, y_{BS}) \longleftarrow$ coordinates of BS;
  $k \longleftarrow \phi_{LOS,AoA}(x_{UE_1}, y_{UE_1})$;
  $i \longleftarrow 1$;
  **while** $P_k < th$ **do**
    $k \longleftarrow k + \frac{1}{4}(-1)^i(2i + (-1)^i - 1)$;
    $i \longleftarrow i + 1$;
  **end**
  **return** $k$
**end**

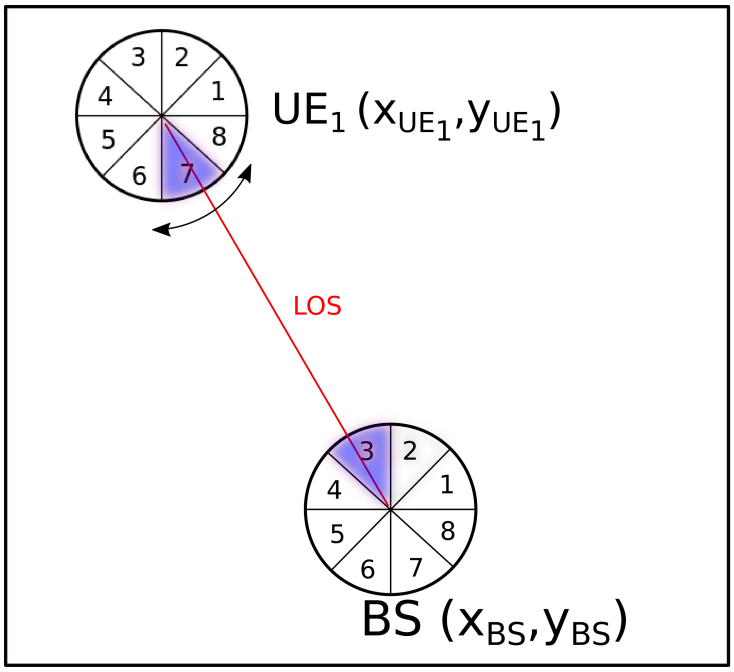


Figure 3.3: LOS Sector Search scenario.

### 3.2.3 Sub-optimal Nearest Neighbour - LOS Mixed Sector Search

This algorithm is a threshold based combination of NN and LOS techniques. We assume that the devices know their position, the position and the sector used by the nearest UE. Moreover we assume that the position of the BS is

known by the UEs and the beam direction used by the BS to communicate with neighbouring UEs (for the AoD case).

The algorithm starts by fetching context information from a legacy network like LTE, then checks the distance between the new UE, $UE_1$, and its nearest neighbour $UE_2$. If the distance is smaller than a threshold $d_{\text{LOW}}$ then the algorithm proceeds like a standard nearest neighbour sector search while if the distance is greater than another threshold, $d_{\text{HIGH}}$, the algorithm carries out a LOS sector search. For distance values included between the two thresholds the algorithm searches sectors in order starting from the most probable. In the next chapter we show how it is possible to compute the analytical probabilities of the angular sectors.

**Algorithm 3:** Nearest Neighbour - LOS Mixed Sector Search.

**Input:** coordinates of BS, coordinates of $UE_2$, active sector of $UE_2$
**Output:** active sector of $UE_1$
**begin**
  $(x_{\text{BS}}, y_{\text{BS}}) \longleftarrow$ coordinates of BS;
  $(x_{\text{UE}_2}, y_{\text{UE}_2}) \longleftarrow$ coordinates of nearest UE;
  $k_{\text{LOS}} \longleftarrow \phi_{\text{LOS,AoA}}(x_{\text{UE}_1}, y_{\text{UE}_1})$;
  $k_{\text{NN}} \longleftarrow$ active sector of $UE_2$;
  $dist \longleftarrow \sqrt{(x_{\text{UE}_1} - x_{\text{UE}_2})^2 + (y_{\text{UE}_1} - y_{\text{UE}_2})^2}$;
  $v \longleftarrow$
   ordered vector with angular sectors probabilities given $[dist, k_{\text{LOS}}, k_{\text{NN}}]$;

  **if** $dist < d_{LOW}$ **then**
    **return** *nearest neighbour sector search*
  **else if** $dist > d_{HIGH}$ **then**
    **return** *LOS sector search*
  **else**
    $i \longleftarrow 1$;
    $k \longleftarrow v(1)$;
    **while** $P_k < th$ **do**
      $k \longleftarrow v(i)$;
      $i \longleftarrow i + 1$;
    **end**
    **return** $k$
  **end**
**end**

The vector $v$ with the angular sectors probabilities in decreasing order is obtained from simulations based on the 3GPP model described in the

previous chapter.

### 3.2.4 Optimal Sector Search

This algorithm is a natural extension of the sub-optimal threshold base sector search. In this case, instead of using the nearest neighbour or the LOS algorithm for certain distance values, the algorithm explores the sectors with decreasing probability of finding the new user, given a) the LOS sector, b) the distance to the nearest user, and c) the sector used by the nearest user. We assume that the devices know their position, the position and the sector used by the nearest UE. Moreover we assume that the position of the BS is known by the UEs. This algorithm further needs the device to have in memory a 4-dimensional matrix where all the possible combinations of nearest neighbour sector, LOS sector, and distance between the two UEs and their relative sector probabilities are stored. The procedure is then simple, the optimal algorithm first fetches all the information it needs and then uses this information to find in the 4-D matrix the relevant ordered sector sequence by which visit the angular space and thus find the right sector to communicate with the BS.

**Algorithm 4:** Optimal Sector Search.

**Input:** coordinates of BS, coordinates of $\mathrm{UE}_2$, active sector of $\mathrm{UE}_2$
**Output:** active sector of $\mathrm{UE}_1$
**begin**
  $(x_{\mathrm{BS}}, y_{\mathrm{BS}}) \longleftarrow$ coordinates of BS;
  $(x_{\mathrm{UE}_2}, y_{\mathrm{UE}_2}) \longleftarrow$ coordinates of nearest UE;
  $k_{\mathrm{LOS}} \longleftarrow \phi_{\mathrm{LOS,AoA}}(x_{\mathrm{UE}_1}, y_{\mathrm{UE}_1})$;
  $k_{\mathrm{NN}} \longleftarrow$ active sector of $\mathrm{UE}_2$;
  $dist \longleftarrow \sqrt{(x_{\mathrm{UE}_1} - x_{\mathrm{UE}_2})^2 + (y_{\mathrm{UE}_1} - y_{\mathrm{UE}_2})^2}$;
  $v \longleftarrow 4D\mathrm{matrix}(k_{\mathrm{NN}}, k_{\mathrm{LOS}}, dist)$  ordered sector vector;
  $i \longleftarrow 1$;
  $k \longleftarrow v(1)$;
  **while** $P_k < th$ **do**
    $k \longleftarrow v(i)$;
    $i \longleftarrow i + 1$;
  **end**
  **return** $k$
**end**

This algorithm determines the sector visit order as a function of nearest neighbour sector, LOS sector and distance between $\mathrm{UE}_1$ and $\mathrm{UE}_2$. The

function that connects the 3 parameters to the best sector visit order is in fact a matrix. In this thesis, the matrix is the result of extensive simulations done for every possible combination of parameters and distances. In order to reduce the matrix size it's possible to exploit cell symmetries and obtain a three dimensional matrix. This is done by using the difference between LOS and NN sector instead of both parameters.

### 3.2.5 Random Sector Search

This algorithm does not require any context information, therefore it does not require any kind of legacy connection nor neighbouring users in order to work. The random sector search provides than upon entering a 5G cell a new UE chooses uniformly randomly a sector where to start the search, it then proceeds in the usual alternative way until it finds a sector with sufficient power level $P_k$ in order to start a connection with the BS. In Fig. 3.4 we outline a scenario representation for the random sector search.

**Algorithm 5:** Random Sector Search.

**Output:** active sector of $UE_1$
**begin**
  $k \longleftarrow$ random sector;
  $i \longleftarrow 1$;
  **while** $P_k < th$ **do**
    $k \longleftarrow k + \frac{1}{4}(-1)^i(2i + (-1)^i - 1)$;
    $i \longleftarrow i + 1$;
  **end**
  **return** $k$
**end**

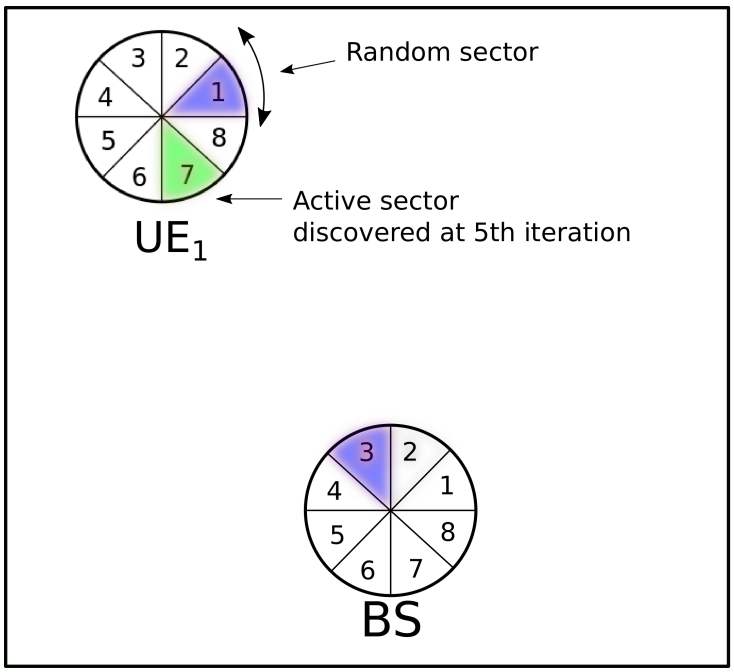


Figure 3.4: Random Sector Search scenario.

# Chapter 4

# Performance Analysis

In this chapter we first derive the probability of two UEs to be in the same sector. Then we use a simulation to verify the results. Lastly we investigate the average time required for a new UE to find the BS sector by exploiting context information provided by the closest UE. First we derive analytically the average discovery time, then we perform a simulation to estimate the average discovery time as function of the distance between two UEs, and finally we perform a simulation to estimate the average discovery time as a function of the number of UEs inside the cell.

## 4.1 Angular Sector Probability

### 4.1.1 Analytical Computation

In this section we compute the probability for a UE to be in the same angular sector, seen by the BS, as another UE. This probability enables us to better understand the relationship between the distance of two different UEs and their active sector.

We start by computing the probability for a new UE to be in sector $i$ given that the nearest UE is in sector $j$, with $i, j \in [1, \ldots, N_{\text{sect}}]$, where $N_{\text{sect}}$ is the total number of angular sectors in which the angular space is divided by each device. We consider the AoA defined in (2.11) for one ray and one cluster $(n, m = 1)$ for two different UEs: 1 and 2. Where the first one is the new UE and the second one has already performed the initial access procedure. Fig. 4.1 shows a top view of the system, where $\text{UE}_1$ is the new device that starts the IA procedure from the same sector as device $\text{UE}_2$ and $N_{\text{sect}} = 8$.

Let $Z_1$ and $Z_2$ be the AoA, as defined in (2.9), of $\text{UE}_1$ and $\text{UE}_2$, respectively. To make the computation more clear we define the difference between

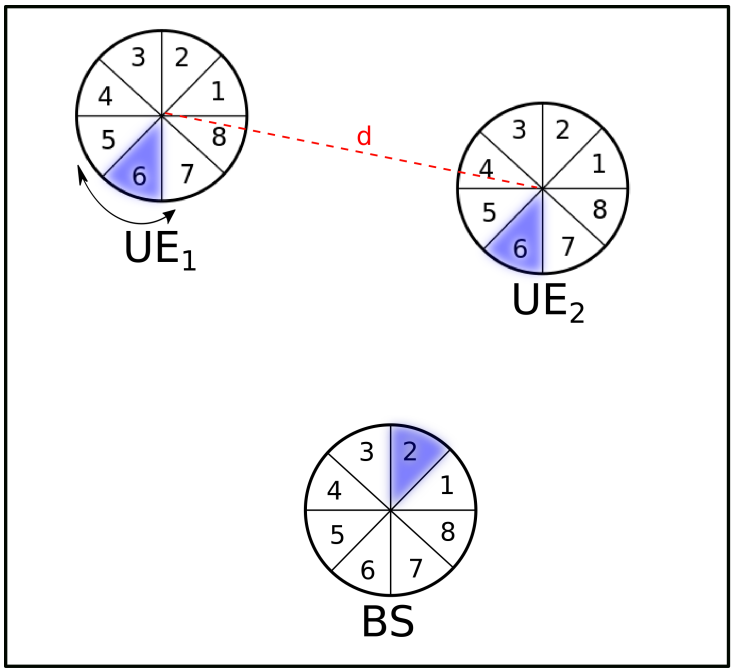


Figure 4.1: System visualization of BS and UEs sectors.

the two angular LOS components:

$$\Delta_{\text{LOS,AoA}} = |\phi_{\text{LOS,AoA}_2} - \phi_{\text{LOS,AoA}_1}|. \tag{4.1}$$

We also define:

$$\gamma = c_{\text{ASA}}\alpha_m. \tag{4.2}$$

From (2.9) and (2.11) we have:

$$Z_1 \sim \mathcal{U}(\alpha, \beta) + \gamma \tag{4.3}$$

$$Z_2 \sim \mathcal{U}(\alpha, \beta) + \Delta_{\text{LOS,AoA}} + \gamma, \tag{4.4}$$

where $\alpha = -10^{\mu_{lgASA}+\sigma_{lgASA}}$, $\beta = 10^{\mu_{lgASA}+\sigma_{lgASA}}$, where $\mu_{lgASA}$ and $\sigma_{lgASA}$ are given by (2.4) and (2.5), and distance between UEs is $d = d_0$. The probability that the AoA of $\text{UE}_1$ is in a given interval $[a_1, b_1]$, given that $\text{UE}_2$ is in the interval $[a_2, b_2]$, is:

$$\begin{aligned} \bar{P} &= P\left[Z_1 \in [a_1, b_1] \mid Z_2 \in [a_2, b_2]\right] \\ &= \frac{P\left[Z_1 \in [a_1, b_1], Z_2 \in [a_2, b_2]\right]}{P\left[Z_2 \in [a_2, b_2]\right]} \\ &= \frac{\beta - \alpha}{b_2 - a_2} \cdot P\left[Z_1 \in [a_1, b_1], Z_2 \in [a_2, b_2]\right]. \end{aligned} \tag{4.5}$$

Where $a_i, b_i \in [0, 360]$ are the angles delimiting the sector we are looking at. Since the AoA of $\mathrm{UE}_1$ and $\mathrm{UE}_2$ are exponentially correlated uniform random variables, we compute probability (4.5) by exploiting the generation of correlated random variables as described in [28]. In particular, $Z_i$ can be obtained as

$$Z_i = F_{Z_i}^{-1}\left(F_{V_i}(v)\right) \quad \text{where} \quad V_i \sim \mathcal{N}(0,1) \tag{4.6}$$
$$F_{V_i}(v) = \Phi(v) = 1 - \mathrm{Q}(v) \tag{4.7}$$
$$F_{Z_i}^{-1}(x) = x(\beta - \alpha) + \alpha, \tag{4.8}$$

and $V_i$ are correlated normal Gaussian random variables. Then (4.5) can be written as

$$\begin{aligned}\bar{P} = \frac{\beta-\alpha}{b_2-a_2} \cdot P[&((1-\mathrm{Q}(v_1))(\beta-\alpha)+\alpha+\gamma) \in [a_1, b_1], \\ &((1-\mathrm{Q}(v_2))(\beta-\alpha)+\alpha+\Delta_{\mathrm{LOS,AoA}}+\gamma) \in [a_2, b_2]].\end{aligned} \tag{4.9}$$

By defining:

$$c_1 = \frac{a_1 - \alpha - \gamma}{\beta - \alpha} \tag{4.10}$$
$$d_1 = \frac{b_1 - \alpha - \gamma}{\beta - \alpha} \tag{4.11}$$
$$c_2 = \frac{a_2 - \alpha - \Delta_{\mathrm{LOS,AoA}} - \gamma}{\beta - \alpha} \tag{4.12}$$
$$d_2 = \frac{b_2 - \alpha - \Delta_{\mathrm{LOS,AoA}} - \gamma}{\beta - \alpha} \tag{4.13}$$
$$\tag{4.14}$$

(4.9) becomes

$$\bar{P} = \frac{\beta-\alpha}{b_2-a_2} \cdot P\left[(1-\mathrm{Q}(v_1)) \in [c_1, d_1], (1-\mathrm{Q}(v_2)) \in [c_2, d_2]\right]. \tag{4.15}$$

Defining

$$e_i = 1 - c_i \tag{4.16}$$
$$f_i = 1 - d_i \tag{4.17}$$

with $i = 1, 2$ we obtain

$$\bar{P} = \frac{\beta-\alpha}{b_2-a_2} \cdot P\left[\mathrm{Q}(v_1) \in [e_1, f_1], \mathrm{Q}(v_2) \in [e_2, f_2]\right] \tag{4.18}$$

and finally

$$\bar{P} = \frac{\beta - \alpha}{b_2 - a_2} \cdot P\left[v_1 \in [\mathrm{Q}^{-1}(e_1), \mathrm{Q}^{-1}(f_1)], v_2 \in [\mathrm{Q}^{-1}(e_2), \mathrm{Q}^{-1}(f_2)]\right]. \quad (4.19)$$

Let $g_i = \mathrm{Q}^{-1}(e_i)$ and $h_i = \mathrm{Q}^{-1}(f_i)$, where $\mathrm{Q}^{-1}(y)$ is the inverse Q function, to get:

$$\bar{P} = \frac{\beta - \alpha}{b_2 - a_2} \cdot \int_{g_2}^{h_2} \int_{g_1}^{h_1} f_{V_1,V_2}(v_1, v_2) dv_1 dv_2 = \quad (4.20)$$

$$\frac{\beta - \alpha}{b_2 - a_2} \cdot \int_{g_2}^{h_2} \int_{g_1}^{h_1} \frac{1}{2\pi\sqrt{1-\rho^2}} \exp\left(-\frac{1}{2(1-\rho^2)}\left(v_1^2 - 2\rho v_1 v_2 + v_2^2\right)\right) dv_1 dv_2 \quad (4.21)$$

where $\rho = e^{-d_0/\Delta_{\mathrm{Corr}}}$ is the correlation coefficient that depends on the distance $d = d_0$. With this procedure we transform random normal Gaussian variables into uniform random variables with an assigned correlation. The integral of equation (4.21) is the probability over a rectangular region and can be computed with the MATLAB function *mvncdf*, multivariate normal cumulative distribution function. The results for AoA NLOS environment and 2 sectors are shown with solid lines in Fig. 4.2 and Fig. 4.3, while the results for AoD are shown in Fig. 4.4 and Fig. 4.5, where each solid line represents a different considered sector for $\mathrm{UE}_1$.

### 4.1.2 Numerical Simulation

We compute the probability of finding two different UEs in the same sector as a function of the distance between them by performing a simulation. In this simulation we generate angles for $\mathrm{UE}_1$ and $\mathrm{UE}_2$ from (4.3) and (4.4) respectively. We generate only the two AoA (or AoD) values for a given distance with the MATLAB function *mvnrnd*. This function, given the right covariance matrix, generates multivariate normal random numbers with the desired exponential correlation. We obtain the probabilities of finding the two UEs in the same sector for every distance and for every number of sector shifts (0 to 63). The results of this simulation, indicated with crosses from Fig. 4.2 to Fig. 4.5, follow the solid line obtained in the analytical computation. Note that some crosses are not perfectly aligned with the analytical lines due to the fact that the sectors at the border of the angular spread are not entirely filled by the angular spread.

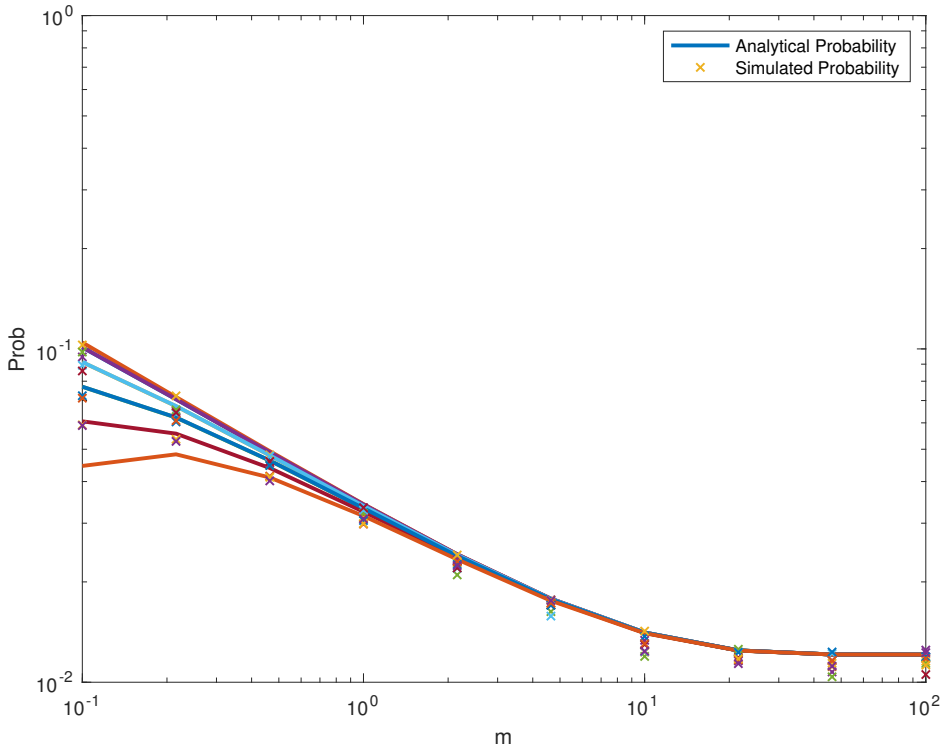


Figure 4.2: Analytical and simulation results for AoA, $f_c = 30$ GHz and $\Delta_{\text{LOS,AoA}} = 0°$.

## 4.2 Average Discovery Time

In this section we compute the expected value of the discovery time for nearest neighbour search approach. Then we perform two numerical simulations: one to evaluate the average discovery time as a function of the distance between two UEs and one to evaluate the average discovery time as a function of the number of UEs present inside the cell. In the simulations we compare the nearest neighbour approach with the random sector search and with the LOS sector search. The random sector search algorithm works as the nearest neighbour search with the only difference that the first sector to be scanned is chosen uniformly randomly between all the possible sectors. Likewise, the LOS sector search algorithm works as the nearest neighbour search with the only difference that the first searched sector is the one corresponding to LOS conditions between BS and UE.

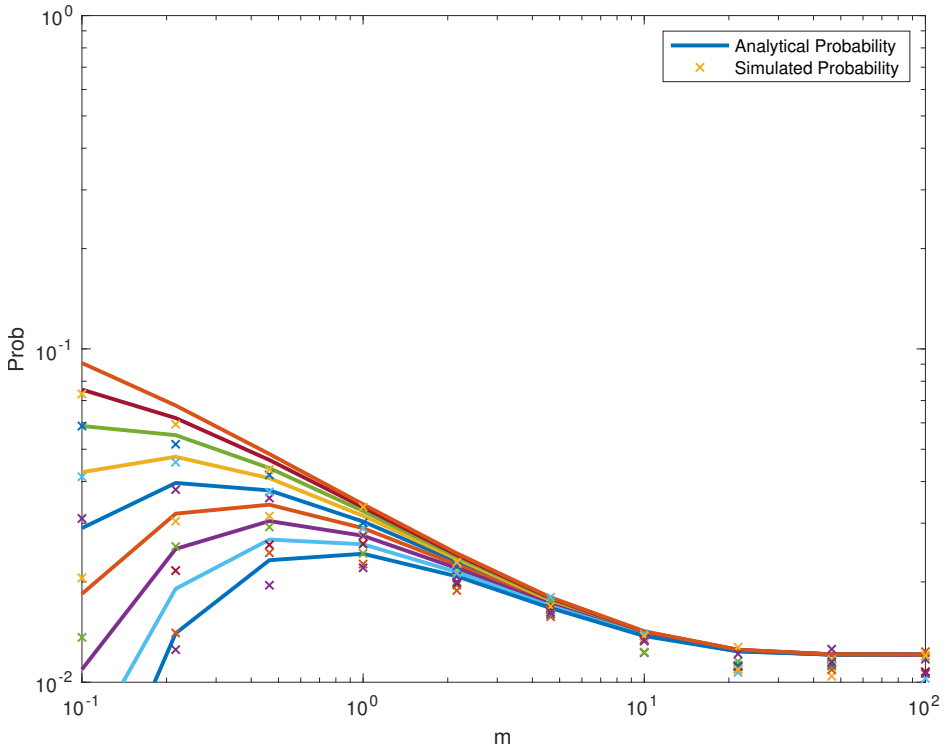


Figure 4.3: Analytical and simulation results for AoA, $f_c = 30$ GHz and $\Delta_{\text{LOS,AoA}} = 40°$.

### 4.2.1 Analytical Computation

In order to compute the expected value of the discovery time we must first define some variables. We call $\tau$ the discovery time, $\tau$ is equal to one when the two UEs are in the same sector. This means that during the IA procedure only one sector has been visited. We define $s_1$ the sector of $\text{UE}_1$ and $s_2$ the sector of its nearest neighbor $\text{UE}_2$. We call $N_s$ the number of sectors in which the angular space is divided and $d$ the distance between $\text{UE}_1$ and $\text{UE}_2$. The average discovery time is

$$\mathbf{E}\left[\tau | d = d_0\right] = \sum_{i=1}^{N_s} i \cdot P(\tau = i | d = d_0) \tag{4.22}$$

where

$$P(\tau = i | d = d_0) = \sum_{k=1}^{N_s} P(s_1 = k + \frac{1}{4}(-1)^i(2i + (-1)^i - 1) | s_2 = k, d = d_0) P(s_2 = k). \tag{4.23}$$

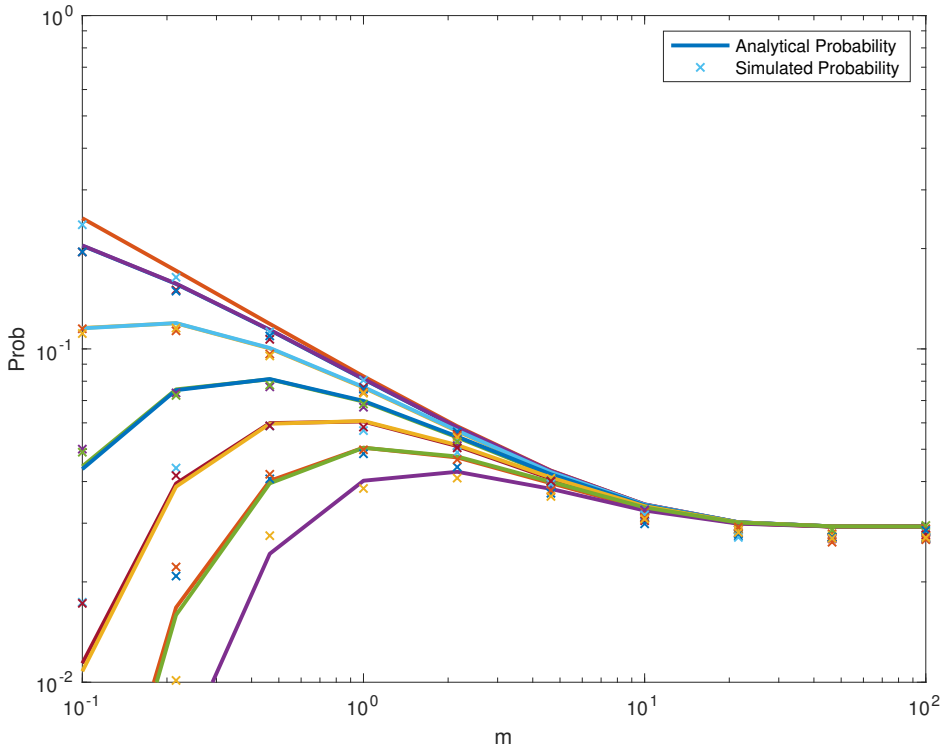


Figure 4.4: Analytical and simulation results for AoD, $f_c = 30$ GHz and $\Delta_{\text{LOS,AoA}} = 0°$.

Defining

$$f(i) = \frac{1}{4}(-1)^i(2i + (-1)^i - 1) \tag{4.24}$$

the function that represents the order of visit for the nearest neighbour search (see Table 4.1), then combining (4.22), (4.23) and (4.24) we obtain

$$\mathbf{E}\left[\tau | d = d_0\right] = \sum_{i=1}^{N_s}\sum_{k=1}^{N_s} \frac{i \cdot P(s_1 = k + f(i), s_2 = k | d = d_0) \cdot P(s_2 = k)}{P(s_2 = k | d = d_0)}. \tag{4.25}$$

Table 4.1: Sector order of visit.

| **i** | 1 | 2 | 3 | 4 | 5 | 6 | 7 | 8 | 9 | 10 | ... |
|---|---|---|---|---|---|---|---|---|---|---|---|
| **f(i)** | 0 | 1 | −1 | 2 | −2 | 3 | −3 | 4 | −4 | 5 | ... |

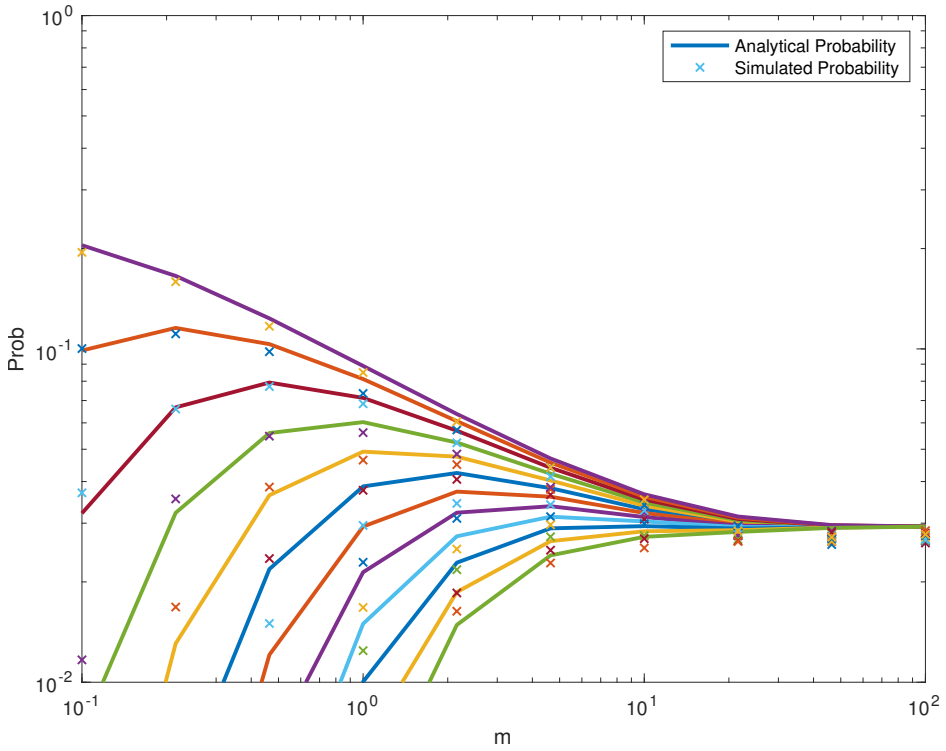


Figure 4.5: Analytical and simulation results for AoD, $f_c = 30$ GHz and $\Delta_{\text{LOS,AoA}} = 40°$.

Since $s_2$ is independent from distance $d$ we get

$$\mathbf{E}\left[\tau | d = d_0\right] = \sum_{i=1}^{N_s} \sum_{k=1}^{N_s} i \cdot P(s_1 = k + f(i), s_2 = k | d = d_0). \tag{4.26}$$

This equation can be analytically computed with a procedure similar to the one described in the previous section that uses the MATLAB function *mvncdf*.

### Analytical Computation Of Optimal Sector Search Vector $v$

In the previous chapter we described the optimal sector search, where a vector $v$ is extracted from a four dimensional matrix. The vector contains the ordered list of most probable angular sectors to visit in order to find the active sector as fast as possible. Indicating, as previously defined in (4.3) and (4.4), $Z_1$ and $Z_2$ the angles of arrival (or departure) of $\text{UE}_1$ and $\text{UE}_2$ respectively, we want to find the angular sector $[a_1, b_1]$ that maximizes the

probability $\bar{P}$ in (4.5) :

$$\arg\max_{[a_1,b_1]} P(Z_1 \in [a_1, b_1] | Z_2 \in [a_2, b_2]). \tag{4.27}$$

Using the results previously obtained in section 4.1.1, we get that (4.27) becomes

$$\arg\max_{[a_1,b_1]} \frac{\beta - \alpha}{b_2 - a_2} \cdot \int_{g_2}^{h_2} \int_{g_1}^{h_1} \frac{1}{2\pi\sqrt{1-\rho^2}} \exp\left(-\frac{(v_1^2 - 2\rho v_1 v_2 + v_2^2)}{2(1-\rho^2)}\right) dv_1 dv_2. \tag{4.28}$$

In this way we compute the first element of the vector $v$. To find the second and the next elements the procedure is the same, we just need to exclude from $[a_1, b_1]$ the sectors found in the previous steps.

### 4.2.2 Numerical Simulation

In the simulations we compute angles of departure for all the different sector search algorithms (nearest neighbour, random, LOS, sub-optimal nearest neighbour-LOS, optimal sector search) and compare them. We provide two different simulations, one where the average discovery time is tested against the distance between two UEs and the other one where the average discovery time is tested against the total number of UEs inside the cell.

#### Average Discovery Time As A Function Of Distance

We simulate a system capable of discriminating $N_s$ sectors, that correspond to $360°/N_s$ degrees for each sector. For every instance of the simulation we generate a new cell with AoD values at each point. Then we place $UE_1$ on the border of the cell and consider as $UE_2$ the UE positioned inside the cell at distance $d$ from $UE_1$ as in Fig. 4.6. This procedure is performed for all the points of the cell border and for distances going from one to a hundred meters. For each pair of differently positioned UEs we perform the nearest neighbor, exhaustive, sub-optimal nearest neighbour-LOS (NN-LOS) and LOS search, looking for the number of sectors visited during each different search procedure. The results can be observed in Fig. 4.7. As we expected the random sector search is independent of the distance between the two UEs and is in fact constant and equal to half the number of sectors $N_s$. Likewise the LOS sector search is independent of the distance between the two UEs and its average discovery time is approximately half the random sector search. We can observe from the figure that the nearest neighbour search outperforms the LOS sector search when the two UEs are closer than 10

meters. For more spatially separate devices the LOS approach outperforms the nearest neighbour. The sub-optimal NN-LOS search, in dashed red line, for distances up to $d < d_{\text{LOW}}$ behaves like the nearest neighbour search, while for $d > d_{\text{HIGH}}$ follows the blue dotted LOS line. Between the two thresholds we can see that combining the two NN and LOS algorithms leads to an overall smaller average discovery time. The optimal sector search by using the results of extensive simulations manages to outperform all the other algorithms in every possible spatial configuration between the UEs.

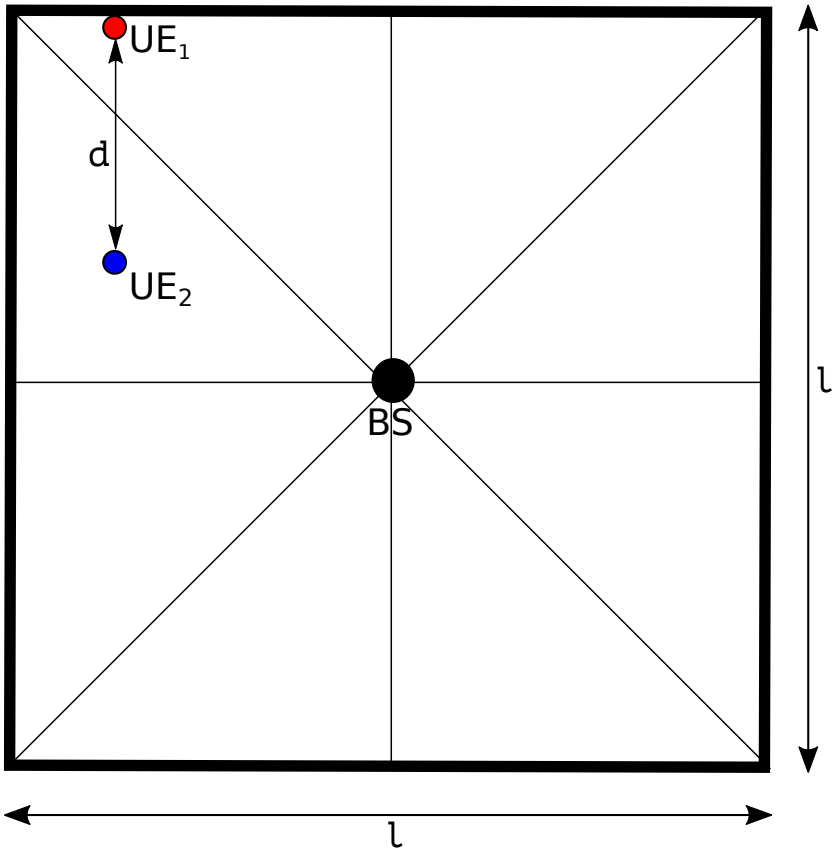


Figure 4.6: Average discovery time simulation as a function of distance setup for $N_s = 8$ sectors.

### Average Discovery Time As A Function Of The Number of UEs Inside The Cell

We now perform a simulation to test the average discovery time behaviour with respect to variations in the number of UEs already present in the cell. The simulation setup is different from the previous one, now we use a circular

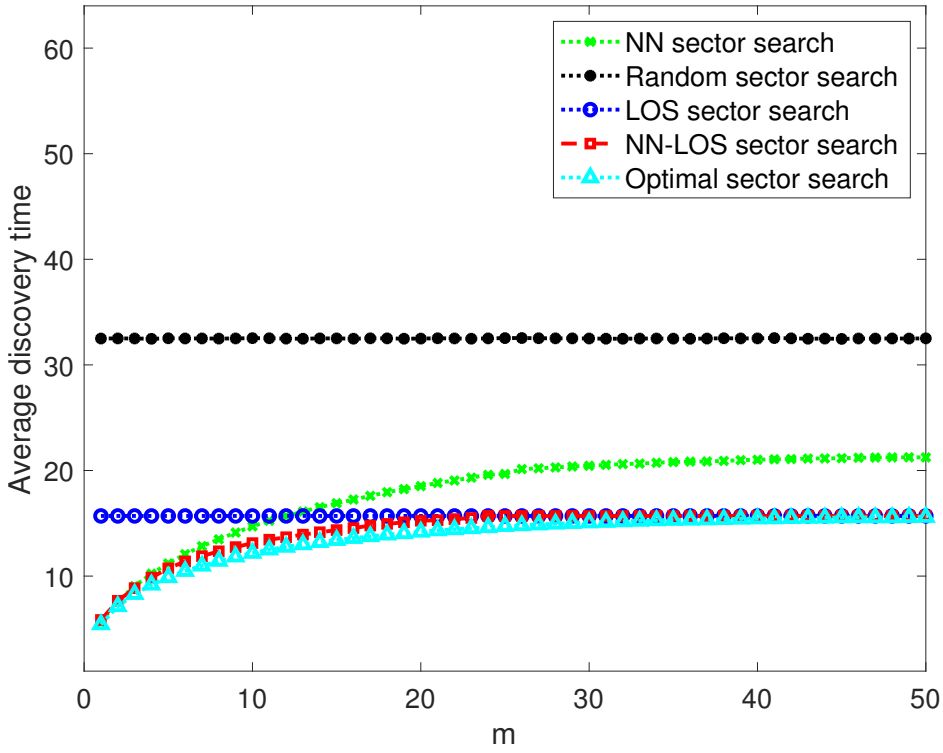


Figure 4.7: Average number of visited sectors for AoD and $f_c = 30$ GHz, $N_s = 64$.

cell with radius $l$ meters, BS located in the center, $N_s$ sectors and $\mathrm{UE}_1$ located at the edge of the cell. The other difference is that now $\mathrm{UE}_2$ is chosen as the nearest UE to $\mathrm{UE}_1$ from a set of size $N_{\mathrm{UE}}$, of uniformly randomly dropped UEs inside the circular cell. The number of randomly dropped UEs, $N_{\mathrm{UE}}$, increases at each iteration from a single UE to 3000 units. In Fig. 4.9 we can observe the result of the simulation for AoD with $N_s = 64$ sectors and cell diameter of $2l = 300$ m. As expected both random and LOS sector search are independent of the number of UEs already present in the cell. We observe that with this particular configuration it is sufficient to have approximately 200 people inside the cell for the nearest neighbour sector search to perform better than the LOS search. In case of very low population density places the LOS approach has a low average discovery time. We observe that the behaviour of the sub-optimal nearest neighbour-LOS sector search, red dashed line, is always better performing with respect to the LOS sector search and the nearest neighbour search. In particular for the lowest density possible is equal to the LOS line and progressively, for high values of UEs it approximates the nearest neighbour behaviour. The

optimal sector search is the overall better performing algorithm. This comes with the price of having to perform a sufficient number of simulations and then storing the resulting matrix.

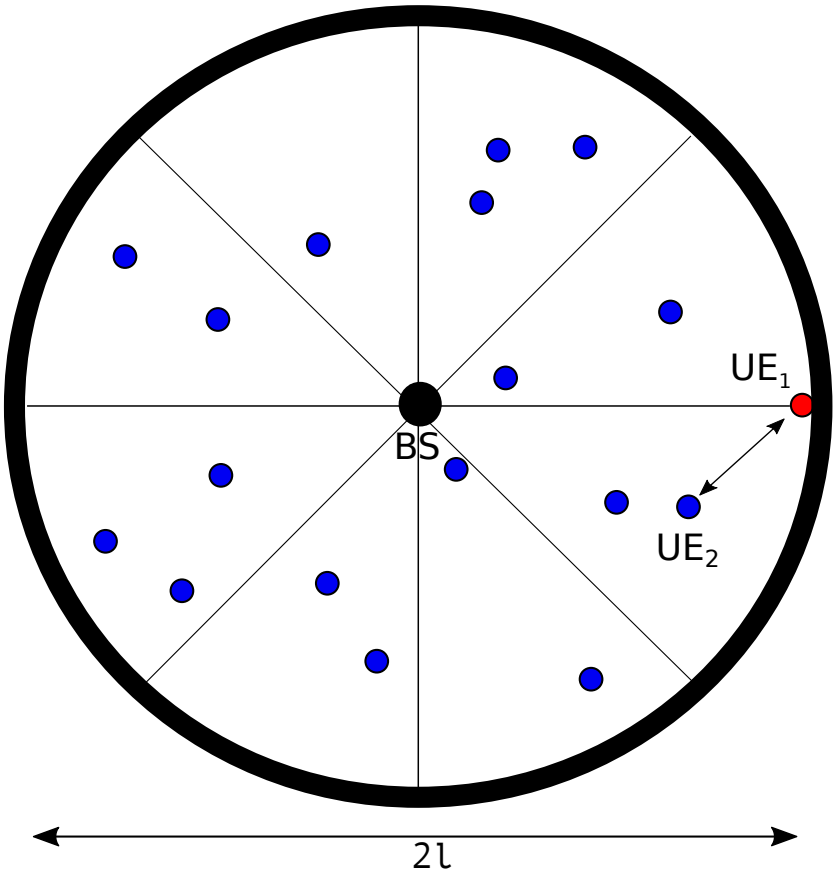


Figure 4.8: Average discovery time simulation as a function of the number of UEs setup for $N_s = 8$ sectors.

## 4.3 Sector Success Probability

In this section we perform a simulation to compare the number of sectors needed to be visited in order to achieve a successful connection between two UEs at a given distance. In Fig. 4.11 sector 0 in the abscissa represents the first sector visited from each of the three (NN, LOS and random search) algorithms, while $1, -1, 2, -2, \ldots$ are the adjacent sectors progressively more distant form the first one. We observe that for short distances (up to 7 meters) the nearest neighbour algorithm achieves better results with respect

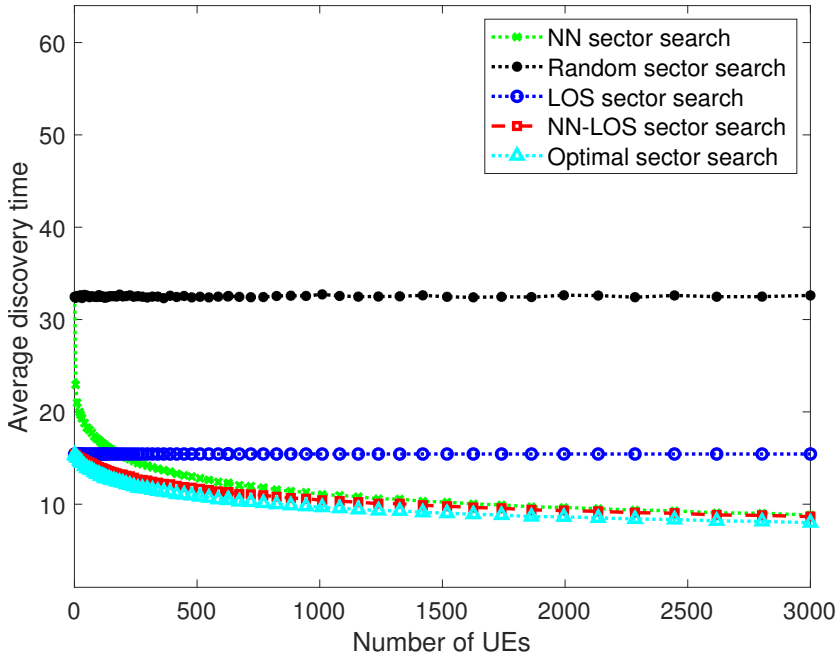


Figure 4.9: Average number of visited sectors for AoD, $f_c = 30$ GHz, $N_s = 64$.

to the LOS and random search algorithms. As expected the random sector search presents a constant behaviour while the LOS sector search shows a peak only for the LOS sector while the adjacent ones show a constant distribution and both are not dependent from the distance $d$ between the two UEs. We observe that the peak in the LOS distribution corresponds to the probability of finding a generic point the 5G cell in LOS condition, see (2.2). For increasing distances $d$, the nearest neighbour search progressively loses the peak in the first visited sector in favour of two smaller peaks symmetric with respect to the first visited sector.

From Fig. 4.15 to Fig. 4.18 we show the cumulative distribution function for different distance values, that is the probability that the number of sectors needed to visit in order to have a successful connection at a given distance is less than a certain value. Despite the low probability of finding the right sector with the first visit (just over 25% in the best case) we can observe how with the nearest neighbour search we reach a 90% probability of finding the right sector to establish a connection between the UE and the BS by searching only 12 sectors, that in this example correspond to searching a circular sector with central angle $\theta = 67.5°$. To achieve the same result with a random sector search in contrast one would need to search a circular sector that spans an angle greater than $\theta = 320°$ while with the LOS sector search

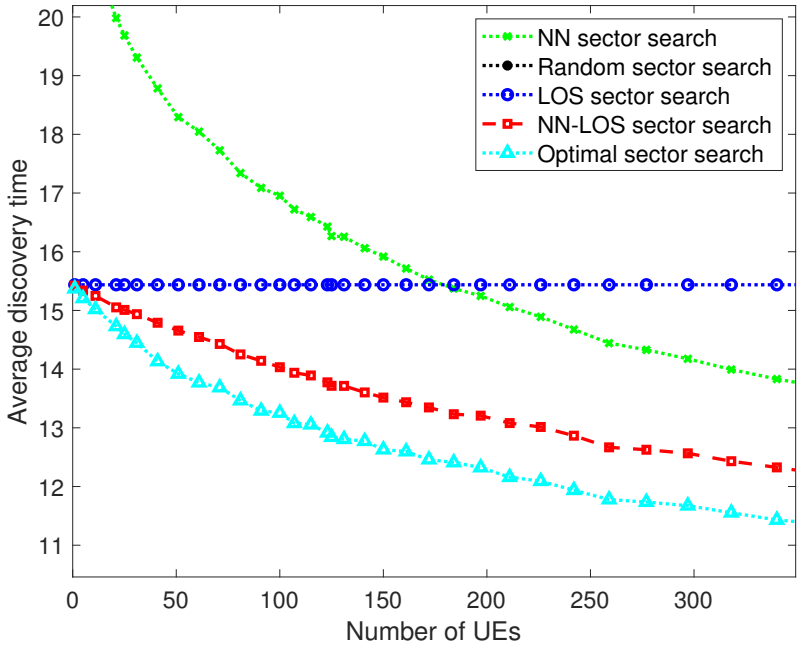


Figure 4.10: Average number of visited sectors for AoD, $f_c = 30$ GHz, $N_s = 64$. Zoom of Fig. 4.9.

the angle would be $\theta = 168^{\circ}$.

From Fig. 4.19 to Fig. 4.23 we show the cumulative distribution function for different numbers of UEs inside the cell. We observe that for a small number of UEs inside the cell the NN sector search is less performing with respect to the LOS, NN-LOS and optimal sector search. With only 5 UEs inside a cell 150 meters in radius the average distance between a newly entered UE and its closest neighbour will be high, thus the correlation between their respective active sectors will be small. For higher number of UEs inside the cell the situation is reversed, and the NN sector search algorithm performance matches the optimal sector search.

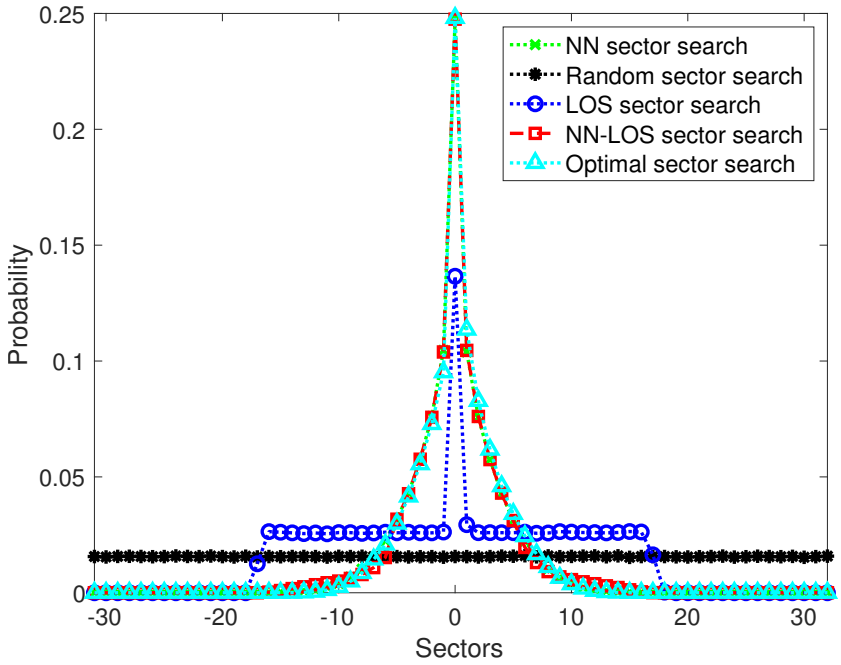


Figure 4.11: Sector Success Probability for AoD, $f_c = 30$ GHz, $N_s = 64$ and distance $d = 1$ m.

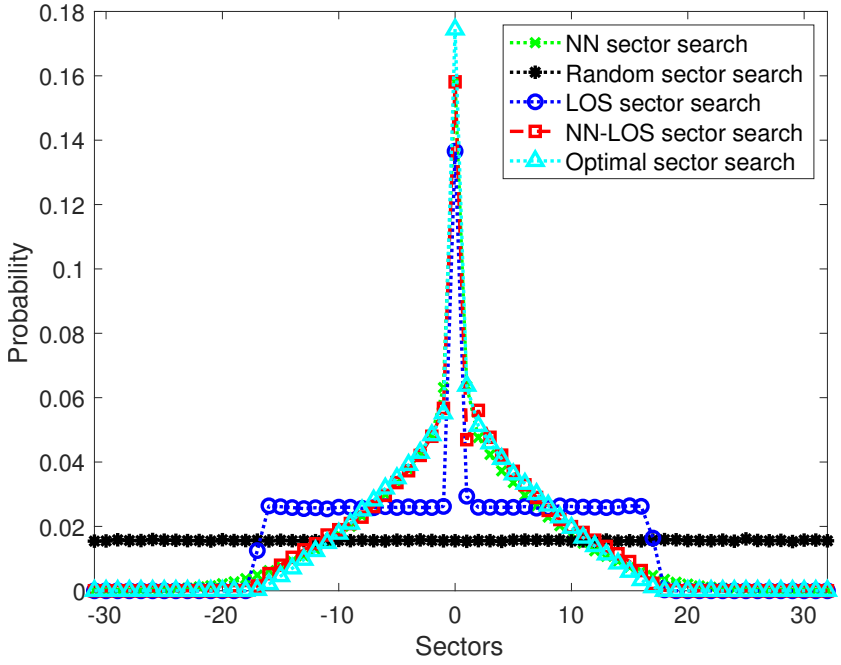


Figure 4.12: Sector Success Probability for AoD, $f_c = 30$ GHz, $N_s = 64$ and distance $d = 5$ m.

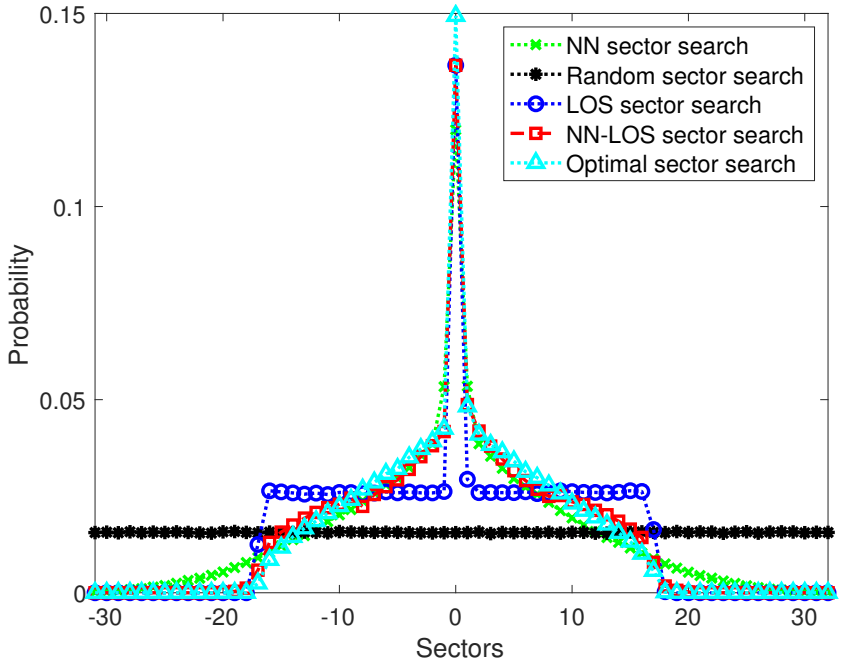


Figure 4.13: Sector Success Probability for AoD, $f_c = 30$ GHz, $N_s = 64$ and distance $d = 10$ m.

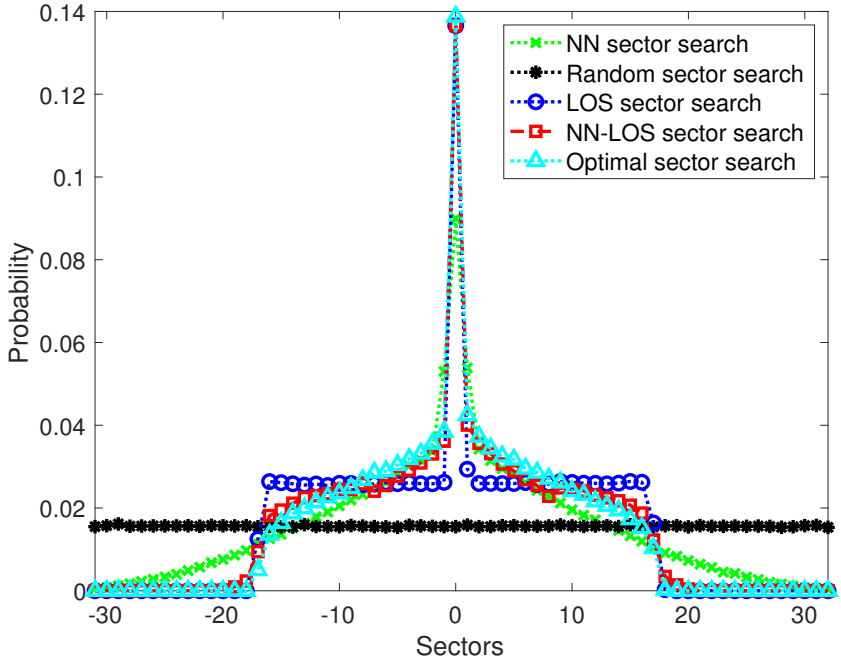


Figure 4.14: Sector Success Probability for AoD, $f_c = 30$ GHz, $N_s = 64$ and distance $d = 15$ m.

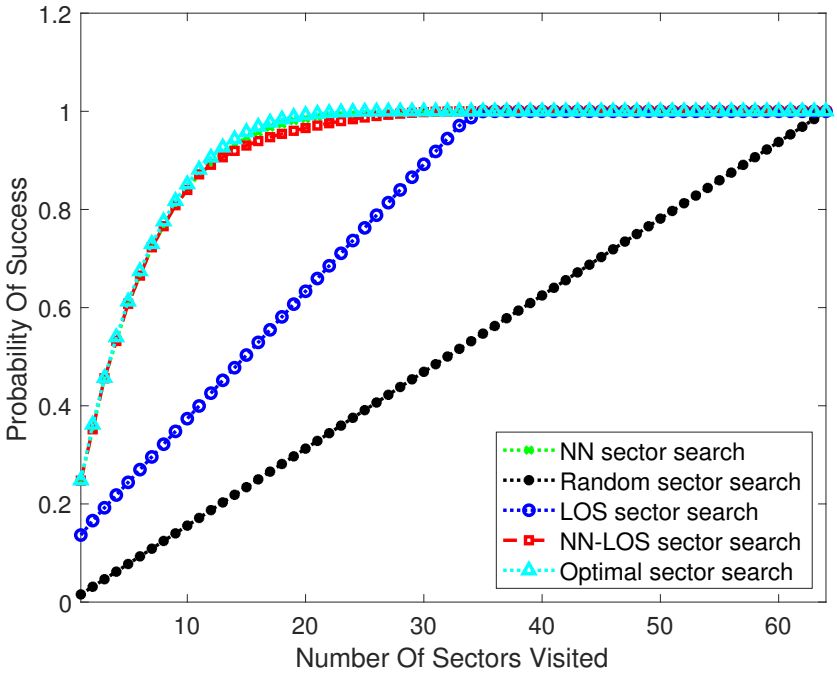


Figure 4.15: Cumulative Distribution Function for AoD, $f_c = 30$ GHz, $N_s = 64$ and distance $d = 1$ m.

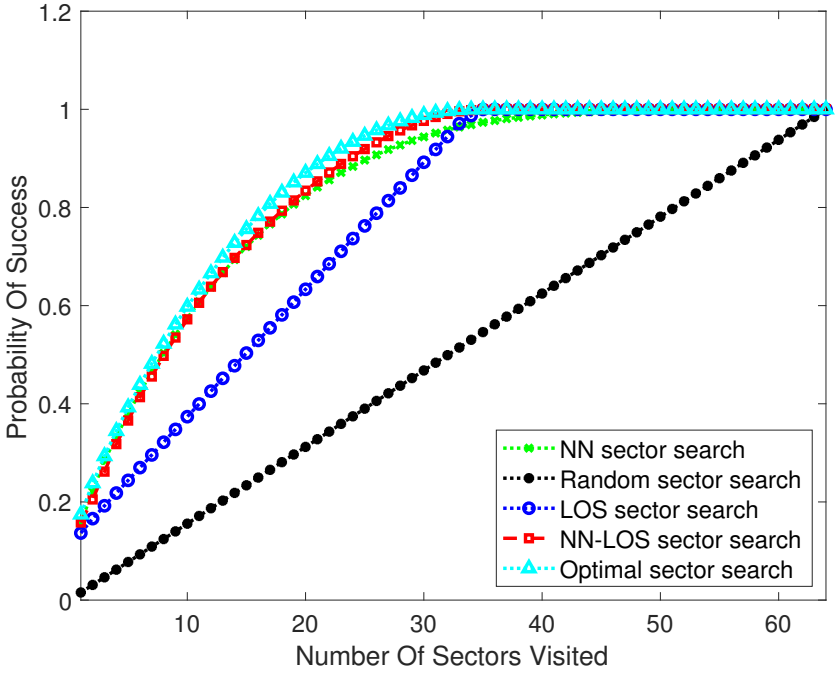


Figure 4.16: Cumulative Distribution Function for AoD, $f_c = 30$ GHz, $N_s = 64$ and distance $d = 5$ m.

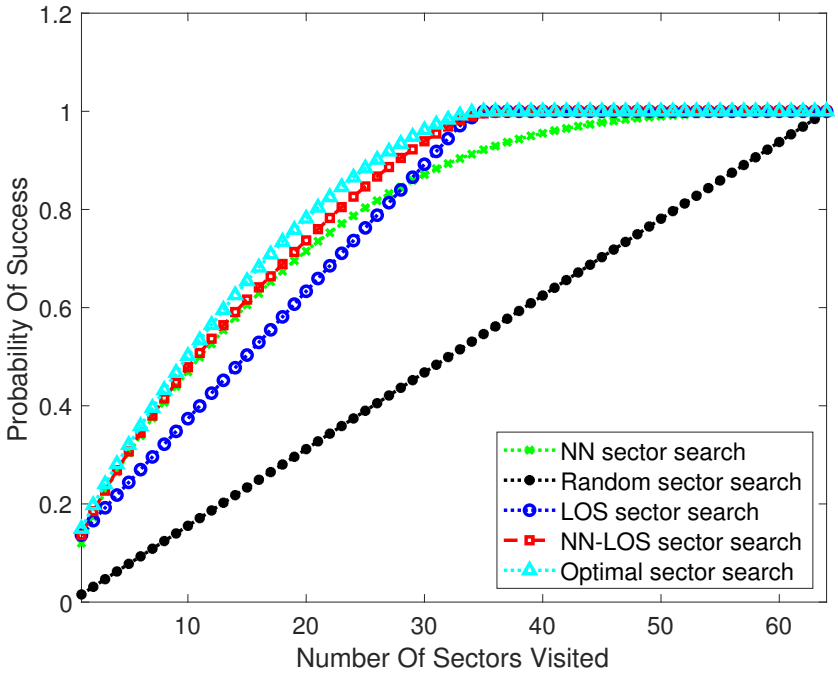


Figure 4.17: Cumulative Distribution Function for AoD, $f_c = 30$ GHz, $N_s = 64$ and distance $d = 10$ m.

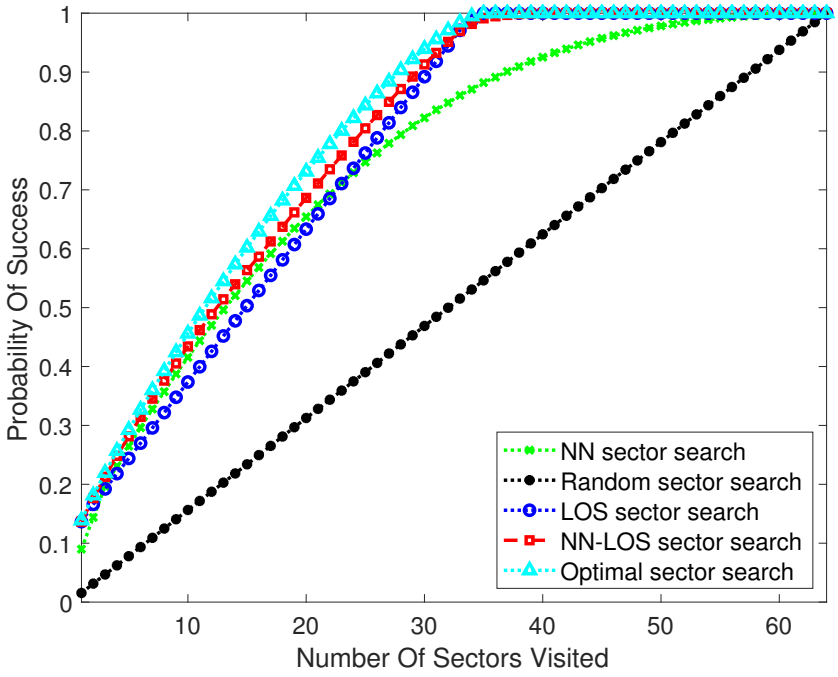


Figure 4.18: Cumulative Distribution Function for AoD, $f_c = 30$ GHz, $N_s = 64$ and distance $d = 15$ m.

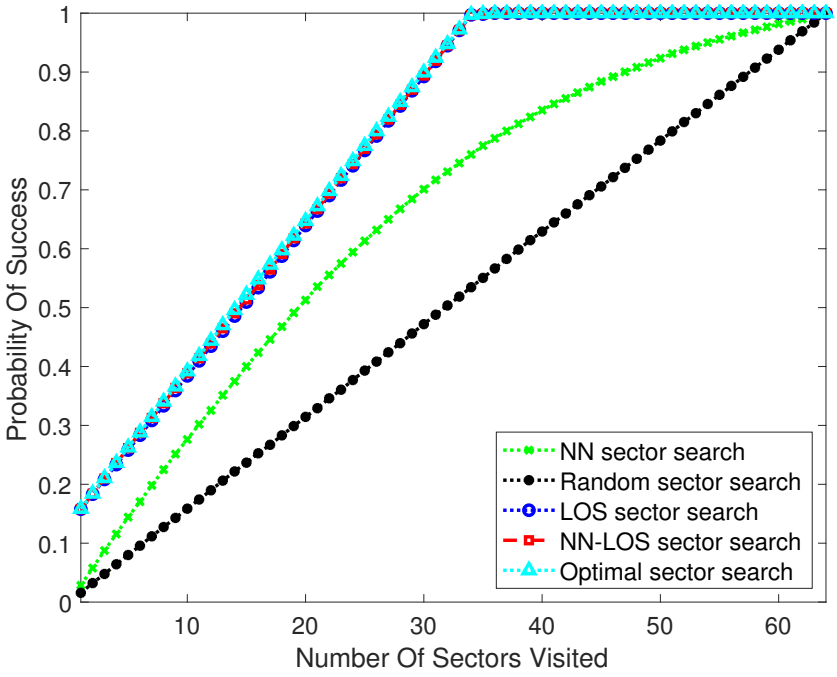


Figure 4.19: Cumulative Distribution Function for AoD, $f_c = 30$ GHz, $N_s = 64$ and 5 UEs.

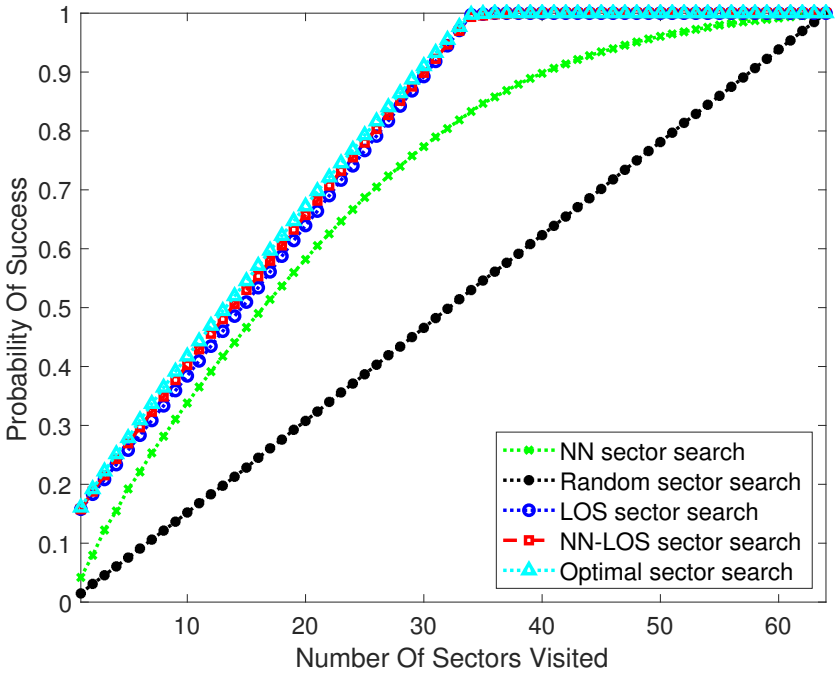


Figure 4.20: Cumulative Distribution Function for AoD, $f_c = 30$ GHz, $N_s = 64$ and 25 UEs.

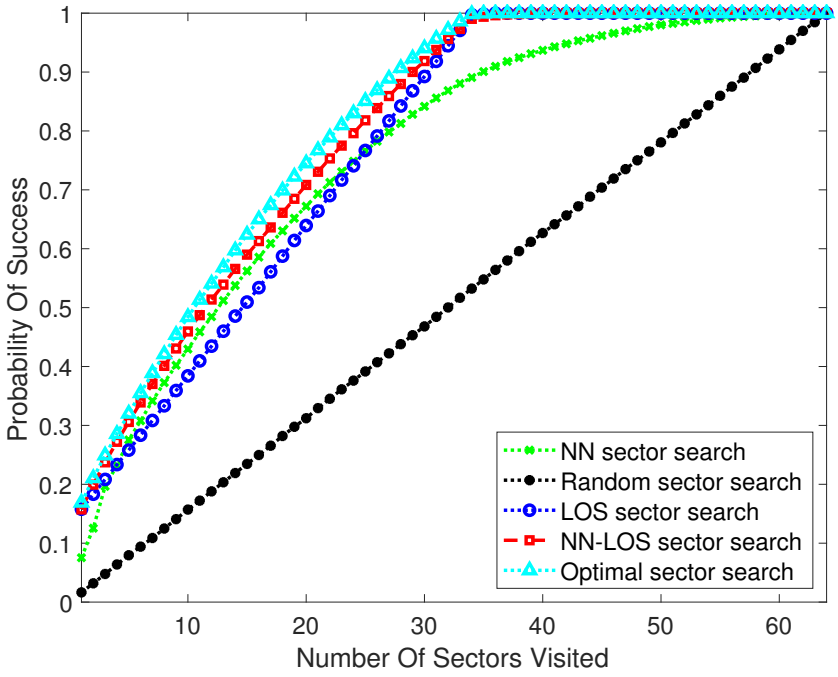


Figure 4.21: Cumulative Distribution Function for AoD, $f_c = 30$ GHz, $N_s = 64$ and 125 UEs.

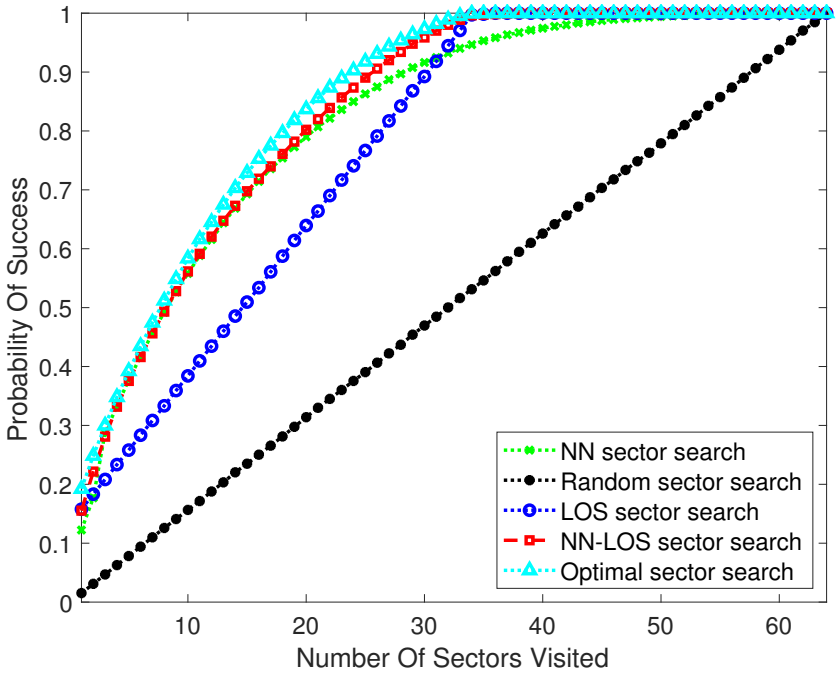


Figure 4.22: Cumulative Distribution Function for AoD, $f_c = 30$ GHz, $N_s = 64$ and 625 UEs.

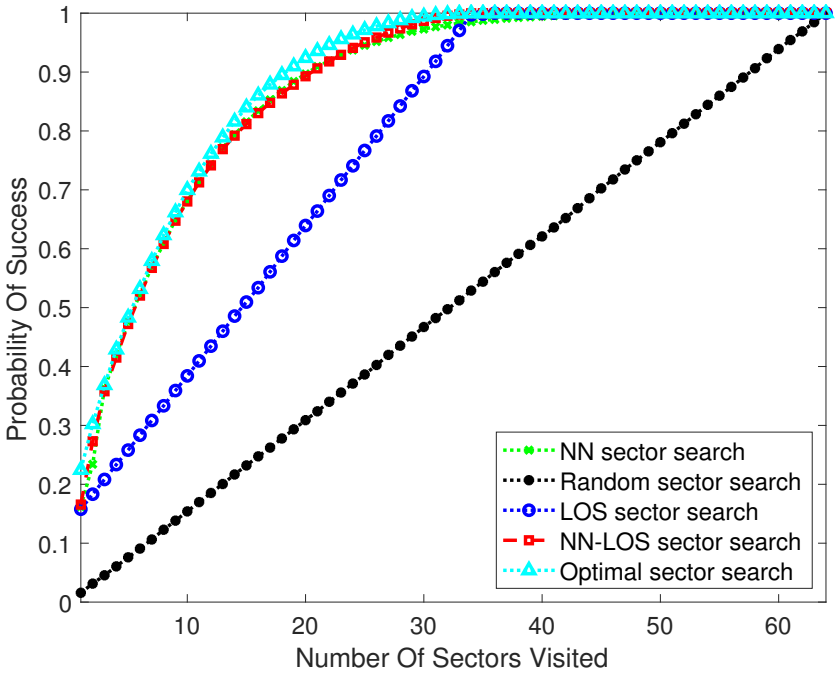


Figure 4.23: Cumulative Distribution Function for AoD, $f_c = 30$ GHz, $N_s = 64$ and 3000 UEs.

# Chapter 5

# Conclusions

In this thesis we have studied and analyzed different possible algorithms to tackle the initial access problem in 5G networks for millimeter wave frequencies.

In the first chapter, after presenting the main 5G goals, we described the 5G new radio access technology, and in particular we focused on the initial access problem. We also provided an overview of the current literature on the 5G initial access techniques, including autonomous search, context-information search, standalone and non-standalone solutions. Then in the second chapter we illustrated the ETSI technical report on the channel model, in particular the spatial consistency procedure, that we later used to simulate the performances of the various algorithms. In the third chapter we described all the IA algorithms we analyzed, mentioning the assumptions and providing the algorithm pseudocode for each case. In the fourth chapter we computed analytically the probability for a UE to use the same angular sector to communicate with the BS, as another UE. Moreover we computed analytically and also by simulation the average discovery time required to perform the initial access procedure for the considered algorithms. In this way we can compare the algorithms performances versus the distances between neighboring UEs or versus the number of UEs present inside the cell. Results show that the optimal sector search is the best performing, this results comes with the con of requiring more context information and memory space to store the 4D matrix. The sub-optimal NN sector search algorithm requires only the active sector of the nearest neighbour as input context information and if used in a place adequately crowded performs very closely to the optimal solution. On the other hand, if the distance between the two UEs becomes too large the algorithm needs more time to find a solution. A compromise between these two algorithms is the sub-optimal NN-LOS sector search that delivers near optimal performances for all the distances between

the two UEs but does not need to store a large 4D matrix in memory.

Since 5G hotspots are expected to be deployed in densely attended areas such as city centers, stations and stadiums where the average distance between people is very low, the NN sector search algorithm could be a key enabler to achieve faster initial access performance.

# Bibliography


[1] E. Dahlman, S. Parkvall, and J. Sköld, *5G NR: The Next Generation Wireless Access Technology*. Academic Press, 2018.

[2] 3GPP, *NR Physical channels and modulation*, 2018. TS 38.211 V15.4.0.

[3] 3GPP, *NR Physical layer procedures for control*, 2018. TS 38.213 V15.4.0.

[4] J. Liu, K. Au, A. Maaref, *et al.*, "Initial access, mobility, and user-centric multi-beam operation in 5G new radio," *IEEE Communications Magazine*, vol. 56, pp. 35 – 41, March 2018.

[5] E. Onggosanusi, M. S. Rahman, L. Guo, *et al.*, "Modular and high-resolution channel state information and beam management for 5G new radio," *IEEE Communications Magazine*, vol. 56, pp. 48 – 55, March 2018.

[6] J. Ryu, "5G/NR - SS Block." https://www.sharetechnote.com/.

[7] X. Lin *et al.*, "5G New Radio: Unveiling the Essentials of the Next Generation Wireless Access Technology," *arXiv:1806.06898*, June 2018.

[8] J. Campos, "Understanding the 5G NR Physical Layer," November 2017. Keysight Technologies.

[9] C. N. Barati, S. A. Hosseini, S. Rangan, P. Liu, T. Korakis, and S. S. Panwar, "Directional cell search for millimeter wave cellular systems," in *Proc. 2014 IEEE 15th International Workshop on Signal Processing Advances in Wireless Communications (SPAWC)*, June 2014.

[10] A. Capone, I. Filippini, V. Sciancalepore, and D. Tremolada, "Obstacle avoidance cell discovery using mm-waves directive antennas in 5g networks," in *Proc. 2015 IEEE 26th Annual International Symposium on Personal, Indoor, and Mobile Radio Communications (PIMRC)*, August 2015.

[11] F. Devoti, I. Filippini, and A. Capone, "Facing the millimeter-wave cell discovery challenge in 5G networks with context-awareness," *IEEE Access*, vol. 4, pp. 8019 – 8034, November 2016.

[12] F. Devoti, I. Filippini, and A. Capone, "Mm-wave initial access: A context information overview," in *2018 IEEE 19th International Symposium on A World of Wireless, Mobile and Multimedia Networks (WoWMoM)*, June 2018.

[13] M. Giordani, M. Mezzavilla, C. N. Barati, S. Rangan, and M. Zorzi, "Comparative analysis of initial access techniques in 5G mmWave cellular networks," in *2016 Annual Conference on Information Science and Systems (CISS)*, March 2016.

[14] M. Giordani, M. Mezzavilla, and M. Zorzi, "Initial access in 5G mmWave cellular networks," *IEEE Communications Magazine*, vol. 54, pp. 40 – 47, November 2016.

[15] W. B. Abbas and M. Zorzi, "Context information based initial cell search for millimeter wave 5G cellular networks," in *Proc. 2016 European Conference on Networks and Communications (EuCNC)*, June 2016.

[16] M. Giordani, M. Polese, A. Roy, D. Castor, and M. Zorzi, "A tutorial on beam management for 3GPP NR at mmWave frequencies," *IEEE Communications Surveys & Tutorials*, vol. 21, pp. 173 – 196, 2019.

[17] M. Giordani, M. Polese, A. Roy, D. Castor, and M. Zorzi, "Initial access frameworks for 3GPP NR at mmWave frequencies," in *2018 17th Annual Mediterranean Ad Hoc Networking Workshop (Med-Hoc-Net)*, June 2018.

[18] M. Giordani, M. Polese, A. Roy, D. Castor, and M. Zorzi, "Standalone and non-standalone beam management for 3GPP NR at mmWaves," *IEEE Communications Magazine*, vol. 57, pp. 123 – 129, April 2019.

[19] H. Soleimani, R. Parada, S. Tomasin, and M. Zorzi, "Statistical approaches for initial access in mmwave 5G systems," in *Proc. European Wireless 2018; 24th European Wireless Conference*, May 2018.

[20] H. Soleimani, R. Parada, S. Tomasin, and M. Zorzi, "Fast initial access for mm-Wave 5G systems with hybrid beamforming using on-line statistics learning," *IEEE Communications Magazine*, August 2019.

[21] C. N. Barati, S. A. Hosseini, S. Rangan, P. Liu, T. Korakis, S. S. Panwar, and T. S. Rappaport, "Directional cell discovery in millimeter wave cellular networks," *IEEE Transactions on Wireless Communications*, vol. 14, pp. 6664 – 6678, December 2015.

[22] C. N. Barati, S. A. Hosseini, M. Mezzavilla, P. Amiri-Eliasi, S. Rangan, T. Korakis, S. S. Panwar, and M. Zorzi, "Directional initial access for millimeter wave cellular systems," in *Proc. 2015 49th Asilomar Conference on Signals, Systems and Computers*, November 2015.

[23] C. N. Barati, S. A. Hosseini, M. Mezzavilla, T. Korakis, S. S. Panwar, S.Rangan, and M. Zorzi, "Initial access in millimeter wave cellular systems," *IEEE Transactions on Wireless Communications*, vol. 15, pp. 7926 – 7940, December 2016.

[24] C. Liu, M. Li, I. B. Collings, S. V. Hanly, and P. Whiting, "Design and analysis of transmit beamforming for millimeter wave base station discovery," *IEEE Transactions on Wireless Communications*, vol. 16, pp. 797 – 811, February 2017.

[25] Y. Li, J. G. Andrews, F. Baccelli, T. D. Novlan, and C. J. Zhang, "Design and analysis of initial access in millimeter wave cellular networks," *IEEE Transactions on Wireless Communications*, vol. 16, pp. 6409 – 6425, October 2017.

[26] A. Pan, T. Zhang, and X. Han, "Location information aided beam allocation algorithm in mmWave massive MIMO systems," in *Proc. 2017 IEEE/CIC International Conference on Communications in China (ICCC)*, October 2017.

[27] 3GPP, *Study on channel model for frequencies from 0.5 to 100 GHz*, 2018. TR 38.901 V15.0.0.

[28] S. T. Li and J. L. Hammond, "Generation of pseudorandom numbers with specified univariate distributions and correlation coefficients," *IEEE Transactions on Systems, Man, and Cybernetics*, vol. 5, pp. 557 – 561, September 1975.

[29] D. De Donno, C. Mazzucco, and S. Tomasin, "Devices and methods for multi-antenna wireless communications," September 2018. Patent filed, nr. PCT/EP2018/075526.

# Acknowledgements

Ringrazio per prime mamma Chiara e nonna Maria che da sempre credono in me e mi sostengono, senza di voi niente sarebbe stato possibile. Ringrazio profondamente Martina che mi supporta e sopporta ogni giorno.

I più sinceri ringraziamenti vanno al mio relatore, Prof. Stefano Tomasin, per avermi dato l'opportunità di affrontare una tesi nell'ambito delle reti di quinta generazione e per avermi dedicato tempo e conoscenza per realizzare al meglio questo lavoro.

Grazie a Cristina che da sempre mi è vicina e continua a sostenermi.

Ringrazio ancora tutti i compagni di questo lungo percorso di studî con i quali ho condiviso intense sessioni d'esame, in particolare: Demir, Beppe, Ivan, Mohammad, Fede, e Roberto.

Desidero infine ringraziare tutti gli amici che rendono questa vita speciale: Cau, Ioni, Lidia, Carlo, Gioia, Alessandro, Daniel, Ambra, Toby, Vale, Pesa, Diego, Leva, Fede, Elena, Davide, Eva.

*Grazie di cuore ad ognuno di voi.*